Chapter 4

VELOCITY FIELD STRUCTURE IN THE ORION NEBULA

4.1 Introduction to the Orion nebula

The Orion Nebula (M42, NGC 1976) is the closest HII region located at a distance of 460pc (Allen, 1973). Embedded in the nebular region are the multiple OB star complexes, θ^1 Ori (Trapezium stars) and θ^2 Ori. The four bright stars in the Trapezium are designated as A, B, C and D in order of right ascension. θ^1 C Ori is supposed to be the principal ionizing source for the nebula with visual magnitude of $\sim$ 5.1 and spectral type O6p. Further, Orion offers maximum surface brightness (emission measure $\sim 8\times10^6$ pc/cm^6, Osterbrock, 1974) and thus providing a good opportunity to study the physical processes taking place in the HII regions in general. Table 4.1

Table 4.1: Ionizing stars in Orion nebula

star	spectral type	T_{eff} K	m_v	radial velocity km/s
θ^1 Ori A	B0.5V	27,000	6.8	24.0
θ^1 Ori B	B3	18,800	8.1	28.0
θ^1 Ori C	O6p	37,500	5.1	33.4
θ^1 Ori D	O9.5V	31,000	6.7	31.0
θ^2 Ori A	O9.5Vp	31,000	5.1	35.6
θ^2 Ori B	B0.5Vp	27,000	6.4	28.5

gives some physical details regarding the prominent stellar sources in Orion.

In this chapter we give details of the results of the observations made on the Orion nebula and discuss the major results obtained. As mentioned earlier, the main aim for the present work has been to understand the velocity field structure over an extended region on the nebula, and to study the velocity field across certain well known features observed in the nebula, viz. the 'bar' ionization front, 'the dark bay' and the molecular cloud region as shown in the Fig 4.1.

Our aim is also to comprehend our results on the velocity field in the light of those on other parameters like density, temperature and intensity obtained using different techniques at different wavelength regions (Infrared: Stacey et al, 1993; Radio: Johnson et al, 1983; and optical: Fischel-Feibelman, 1973, Pogge et al, 1992). Further, the recent optical images of the nebula

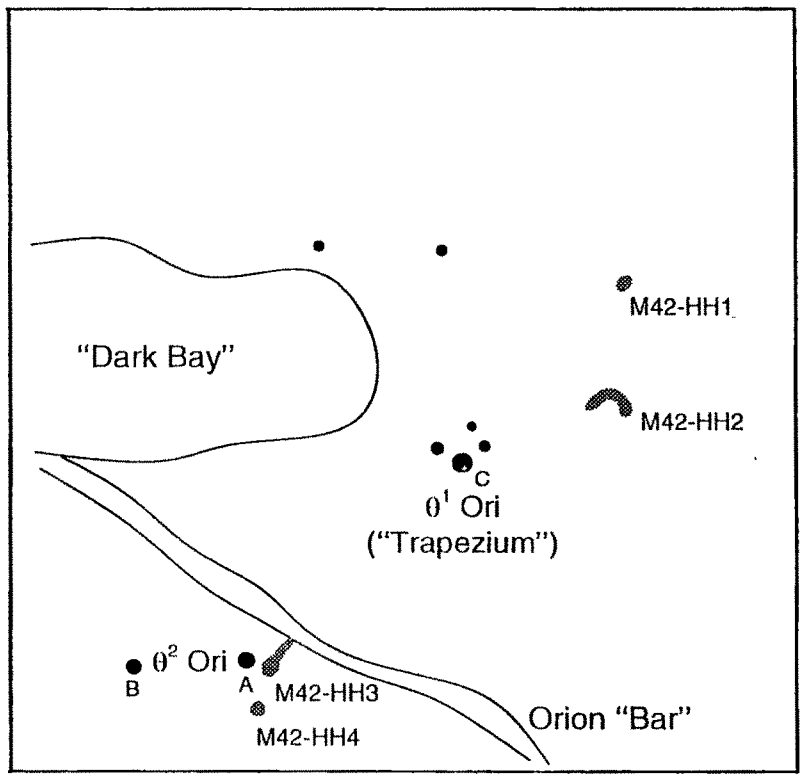

Figure 4.1: A schematic of Orion nebula, M42 showing important features(adapted from Pogge et al, 1992)

obtained by Hubble space telescope (Hester et al, 1991) at the high spatial resolution resolved some more new sources (viz. jets, HH objects) which were not detected in earlier studies due to the lack of adequate resolution. Therefore it is our attempt to understand the kinematics of the gas about these features. In this chapter we discuss in detail the present work with a brief description of the studies made in the past on the Orion nebula.

4.2 Earlier studies

4.2.1 Kinematics

In the past, several studies have been made to determine the radial velocity structure of the brighter portions of the Orion Nebula. The earliest and the most detailed kinematic studies were made by Wilson et al (1959). They observed the emission lines of [OIII] 5007 Å, [OII] 3726 Å and Hγ 4340 Å using multi-slit spectroscopy covering the central bright portion of about $4' \times 4'$ around Trapezium stars. They have shown that there was variation of widths and structures of the lines across the Nebula and also splitting of [OII] and [OIII] lines was observed in certain regions. Spectroscopic observations by Meaburn(1977) also showed splitting of [NII] line in certain regions. More studies made by using Fabry-Pérot Spectrometer (Meaburn 1971; Goudis and Balick 1980; Hippelein and Munch 1983; Smith and Weedman 1970; Dopita et al, 1973; Hanel, 1987) and echelle systems (Fountain el al, 1979; Hufson et al, 1981; Clayton et al, 1985; Meaburn, 1984) showed that the velocity field

structure in the Orion nebula is very complex. Spectroscopic observations were also made at other wavelengths like radio (Pankonin et al 1979, Goudis et al, 1984) and infrared wavelenghs (Stacey et al, 1991; Genzel et al, 1989). As mentioned earlier, these studies did not have adequate spatial or spectral resolution or were limited by the instrument used (i.e., slit spectroscopy). The high spatial and spectral resolution studies made by Castañeda covered only limited regions (along the length of the slit) especially around θ^2 A Ori. In the present studies these problems are overcome by making observations on an extented region with reasonably good spatial and spectral resolution.

4.2.2 Turbulence

von Hoerner (1951) was the first to attempt an interpretation of the random motions observed in Orion in terms of turbulence using the data of Campbell and Moore (1918). His studies showed that the standard Kolmogorov relation for the Structure function, $B(r) \propto r^{\frac{2}{3}}$ was satisfied. Later attempts were made by Courtes (1955) and Pikel'ner and Shain(1954). But the quality of their data did not allow for any definite conclusion.

It was Munch (1958) who then using the data of Wilson et al (1959) studied the turbulent motions of Orion and found that the Kolmogorov relation was not satisfied. He argued that the failure of the Kolmogorov law could be due to the presence of compressibility of the nebular gas. But, some doubts were raised much later (Castañeda, 1988) since the analysis was based on

selecting the maximum intensity values without considering the shape of the line profile or accounting for multiple velocity components which could be possibly present in the profile. Castañeda's recent analysis with high resolution of the structure function for the study of turbulence showed variation with the size parameter in the value of the expected slope (0.66). It was argued that this could be due to the energy source driving the turbulence being input at several scales.

With the large number of well distributed data points obtained in our obervations, a better estimate of the statistical functions can be made for the sudy of turbulent motions.

4.3 Present studies

Fig. 4.2 shows a mosaic of four interferograms on the Orion at different etalon gap spacings. As mentioned earlier a total of 33 interferograms were used in the data analysis. Firstly, the kinematic information in a region was extracted from the observed interferograms as described in section 3.2. Velocity profiles were obtained for about 2000 positions on the nebula. The velocity field was studied in three aspects: (i) General velocity flow due to expansion of the HII region; (ii) High velocity flows associated with different physical processes taking place in the nebula and (iii) Random or turbulent flow. In what follows, we describe our results on these three aspects and discuss their implications.

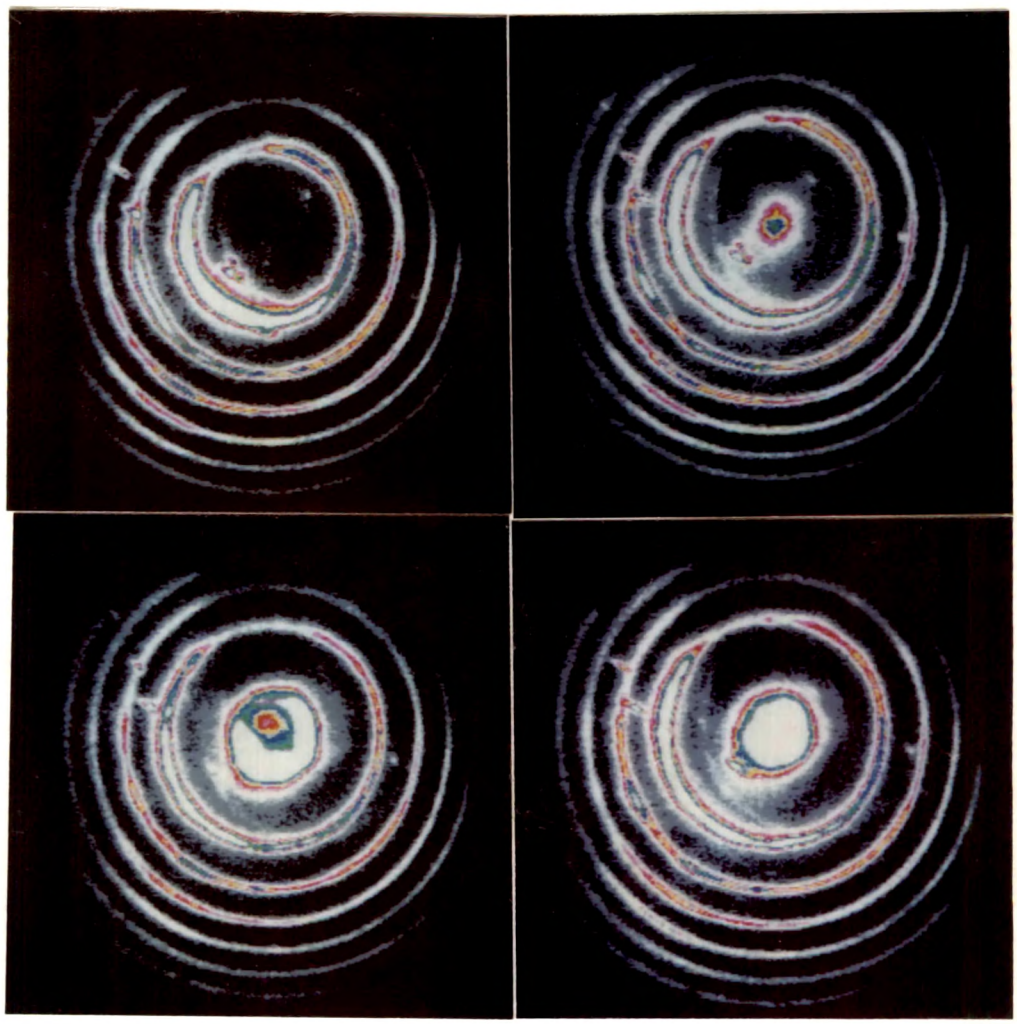

Figure 4.2: A mosaic of four interferograms of the Orion nebula in [OIII] 5007 Å line taken at different increasing étalon spacings. The expansion of the fringe pattern as the étalon is scanned can be noted.

4.4 General velocity flow

4.4.1 Two components

By visual inspection , in general, the profiles are found to be either asymmetric or broad winged. Therefore, in general two gaussians were necessary to fit the profiles: a narrow one and a broad one. In most cases, the FWHM of the narrow component was found to be about 20 $\pm$ 3 km/s and that of broad component was about 50 $\pm$ 3 km/s. It is seen that the broad component is either blue-shifted or red-shifted with respect to the narrow profile as shown in Figs. 4.3 and 4.4 respectively.

In some positions it matches with the peak of the narrow component as shown in Fig. 4.5. It is also observed that the amplitude of the broad profile varies with respect to the narrow profile, as shown, for instance, in Fig. 4.6 which shows a stronger broad component.

Since profiles can be obtained using the Imaging Fabry-Pérot Spectrometer either by taking radial scans at any spatial point on a given fringe or by scanning the FP etalons over one FSR and obtaining profiles at any given pixel, we have identified more than 100 pixels where the scanning had provided complete profiles. The velocity profiles at these positions were generated and fitted with appropriate gaussians. It was found that here also two gaussian components could be fitted for most of these profiles, an example of which is given in Fig. 4.7. The FWHM of the two components are found to

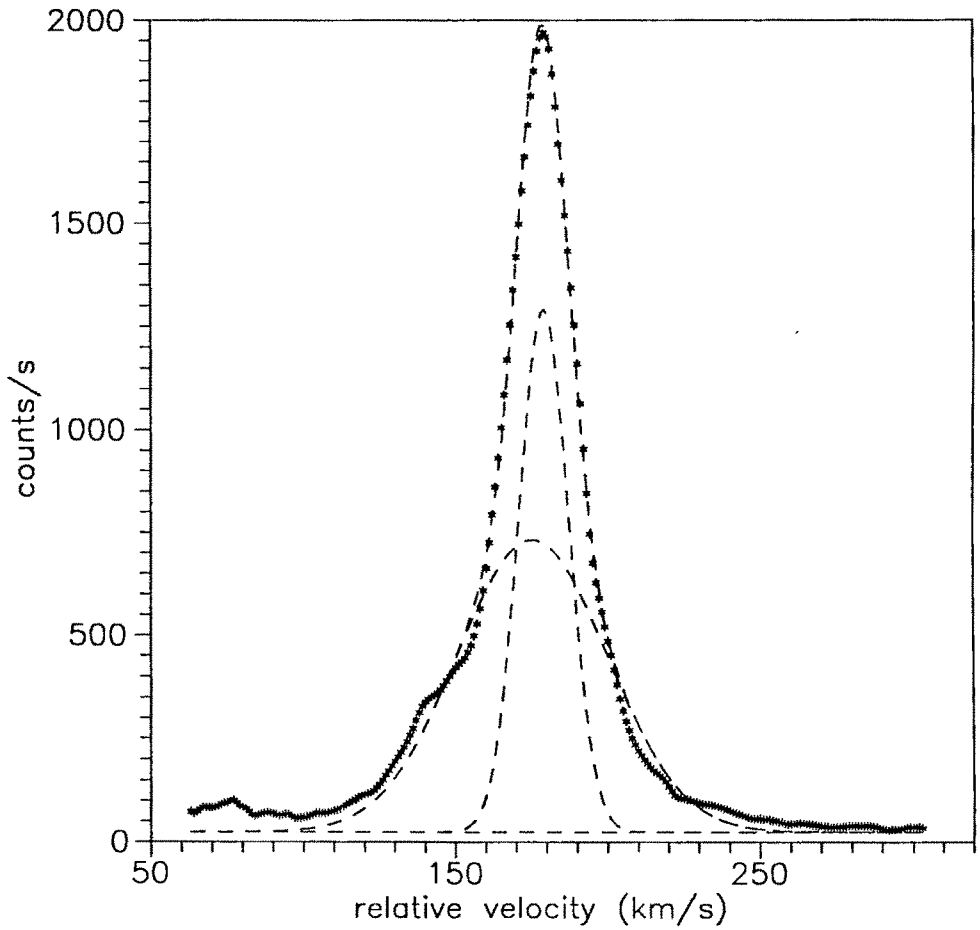

Figure 4.3: Line profile showing asymmetry (data points are denoted by asterisks). The dashed curve going through the asterisks is the composite gaussian fit with the individual gaussians shown by the small dashed curves. The dashed line at the bottom is the continuum level. The broad-component is blue-shifted with respect to the narrow one.

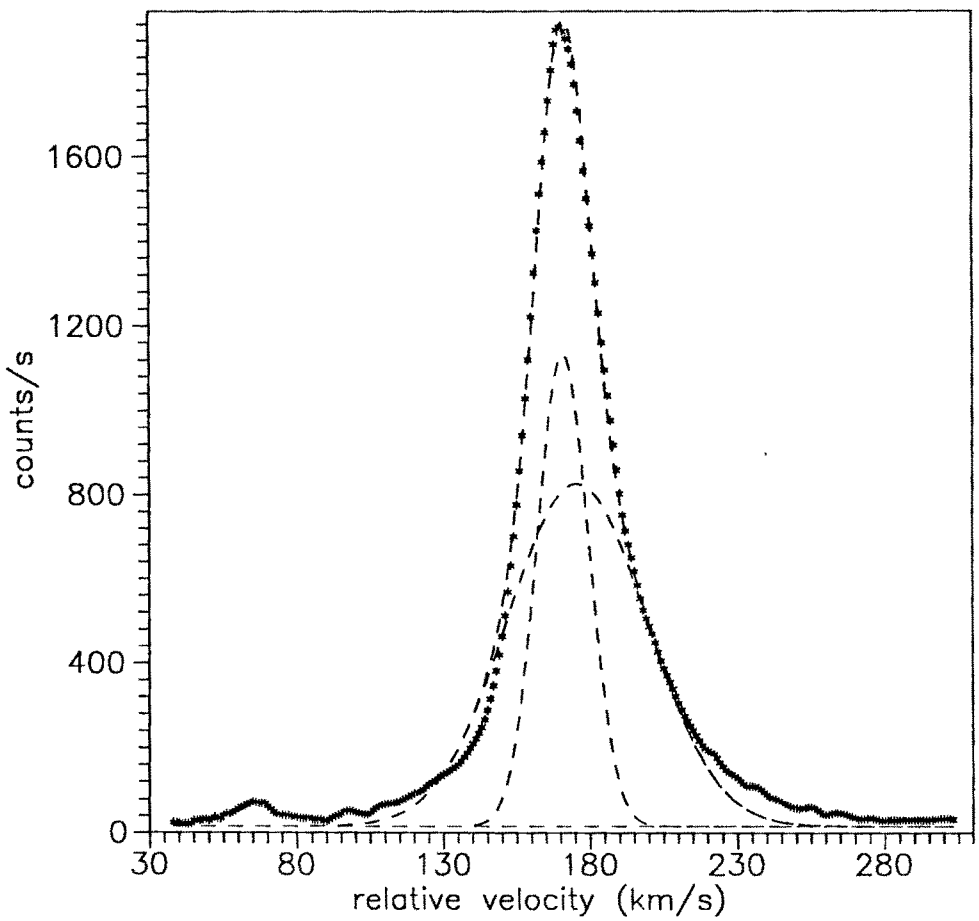

Figure 4.4: Line profile showing asymmetry (data points are denoted by asterisks). The dashed curve going through the asterisks is the composite gaussian fit with the individual gaussians shown by the small dashed curves. The dashed line at the bottom is the continuum level. The broad-component is red- shifted with respect to the narrow one.

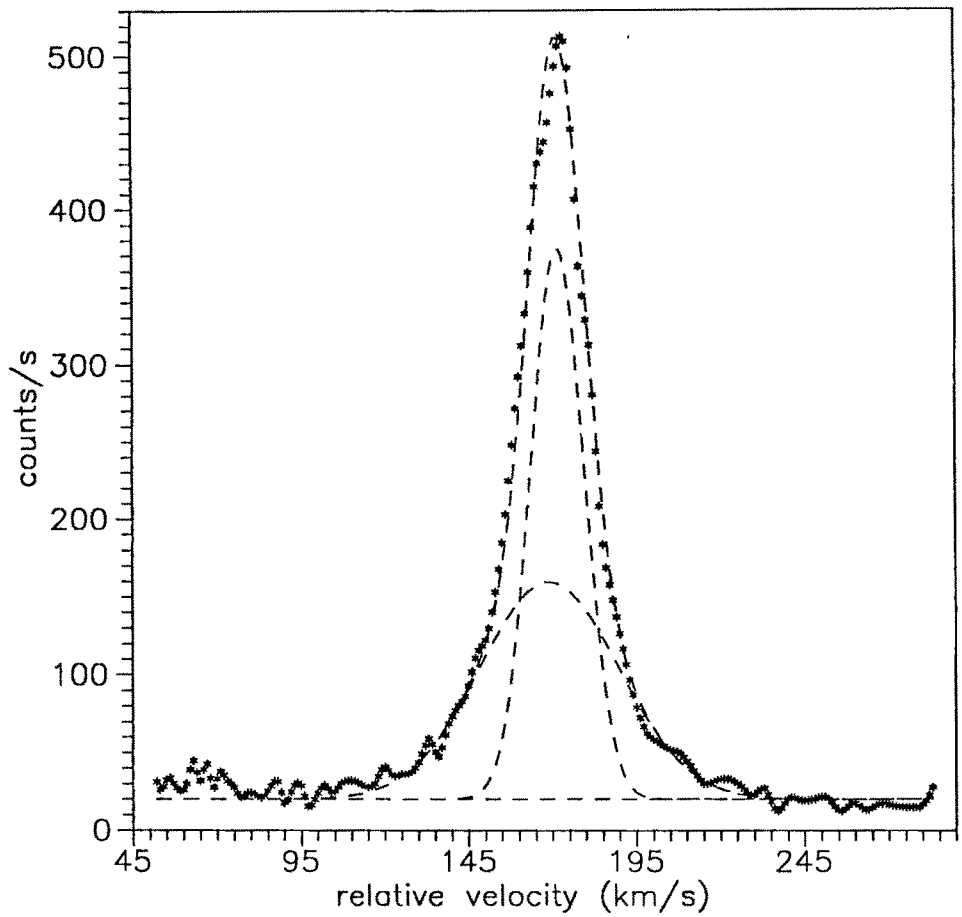

Figure 4.5: Line profile showing broad wings(data points are denoted by asterisks). The dashed curve going through the asterisks is the composite gaussian fit with the individual gaussians shown by the small dashed curves. The dashed line at the bottom is the continuum level. The broad-component and the narrow one have no relative velocity.

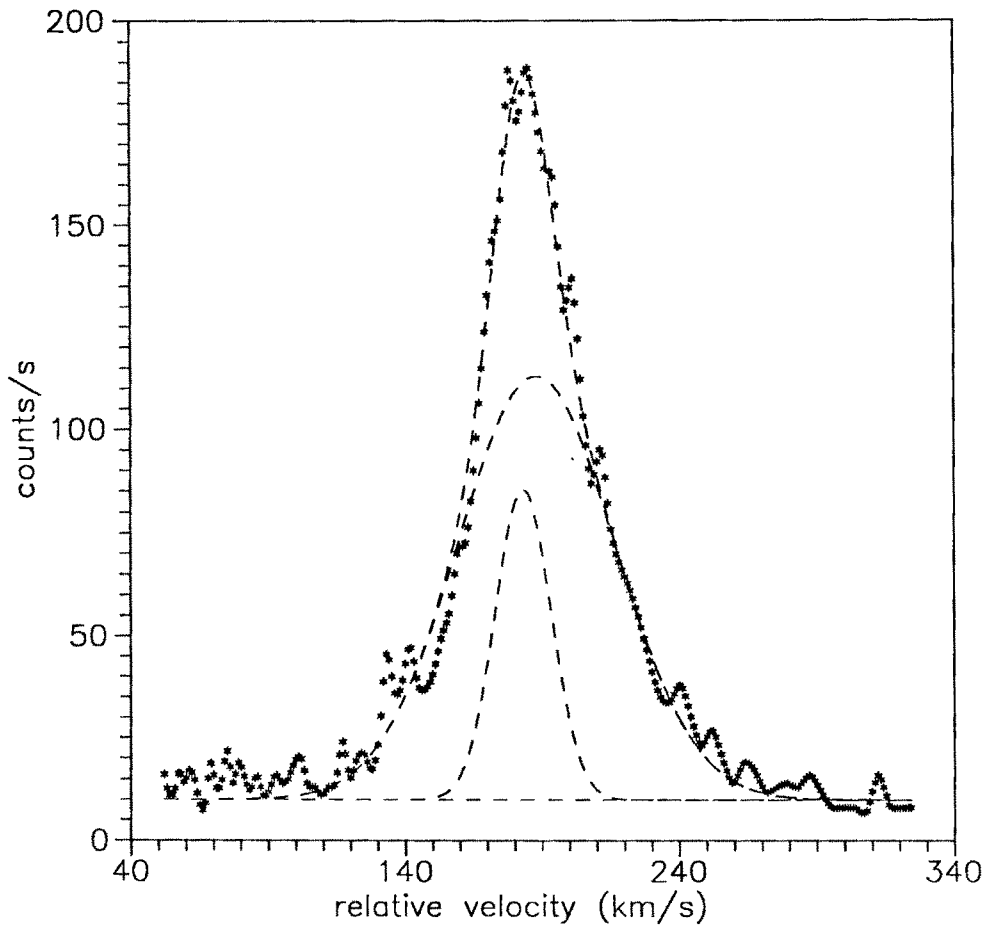

Figure 4.6: Line profile showing broad wings(data points are denoted by asterisks). The dashed curve going through the asterisks is the composite gaussian fit with the individual gaussians shown by the small dashed curves. The dashed line at the bottom is the continuum level. The broad component is stronger then the narrow one.

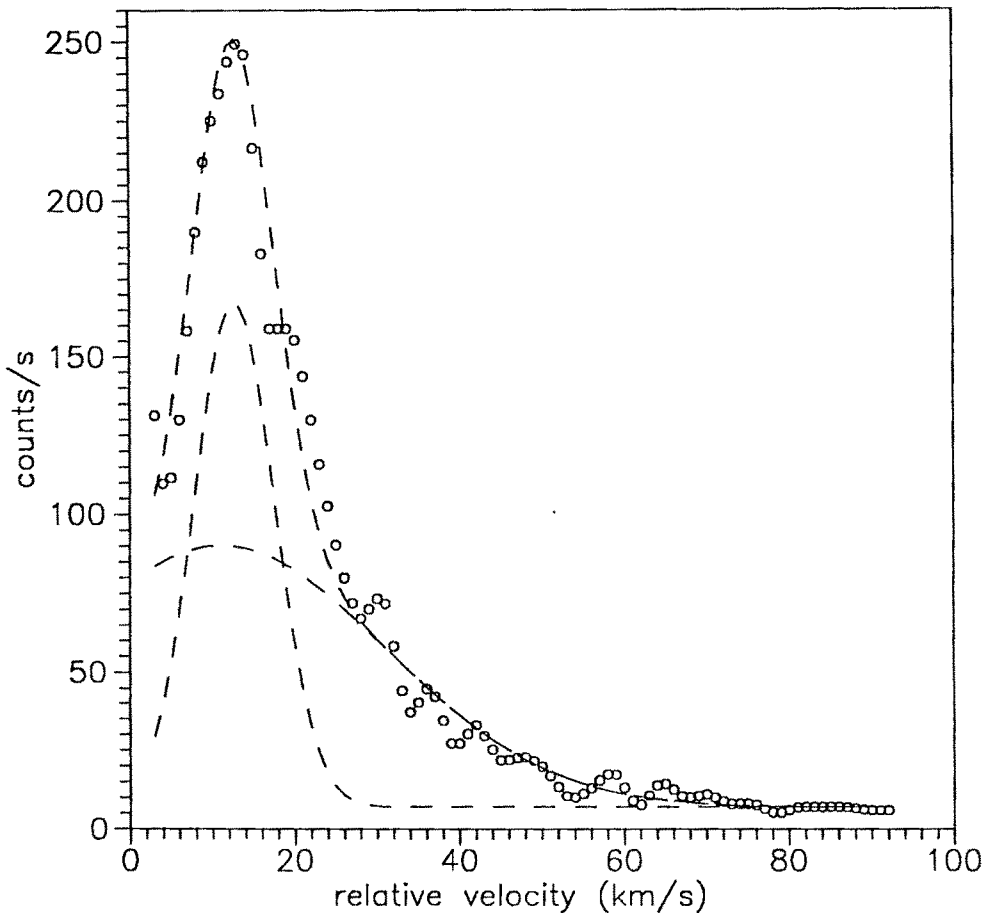

Figure 4.7: Line profile at a single pixel (data points are shown by circles) fitted with two gaussians.

be about (i)15 $\pm$ 3 km/s and (ii)50 $\pm$3 km/s at a position (1.8′N, 52″W of Trapezium), showing a very good correspondence with the results obtained from the radial scans.

It should then be seen if these two components actually represent two different flow patterns or these are created artificially. The latter possibility may arise (i)due to the uncertainity in the gaussian fitting procedure (ii)because the gaussian fitting is actually forced and (iii)because of the fact that we did not deconvolve the observed profiles for the instrumental broadening. As mentioned earlier, the uncertainity in the gaussian fitting procedure is about 10% for a good S/N ratio and as such cannot account for the second amplitude by itself; also, the fit was very bad with just one gaussian, implying therefore that there have to be two components to explain the observations. As far as the forcing of the gaussian fit is concerned, the reason lies in the physical aspects of the line profile in the diffuse nebula: the thermal broadening and the turbulence are gaussians and the velocity gradient does not change the profile shape selectively in the wings. The broadening of the wings due to pressure effects is not relevant in the nebular conditions. To check the instrumental broadening the profile at a single pixel was deconvoled and then fitted with gaussians (Fig. 4.8). The fit seems to be quite good implying that it is not the effect of the instrument. Finally, this leaves us with the possibly inevitable result that there, in fact, might be multiple components.

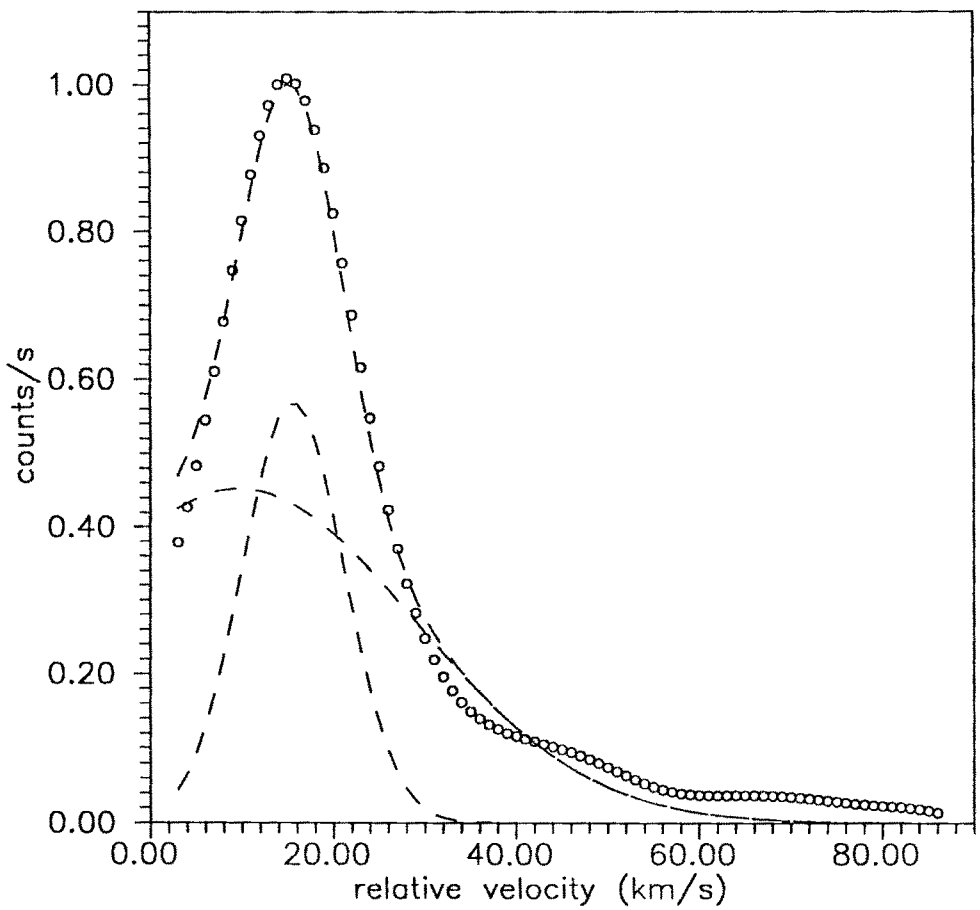

Figure 4.8: Deconvolved profile of the line profile at a single pixel(shown in Fig. 4.7) fitted with two gaussians.

4.4.2 Discussion

In the Orion nebula, according to the broadly accepted model (Balick et al, 1980), θ^1 C Ori ionizes the gas resulting in the formation of a 'core' of ionized gas. The dense neutral cloud situated behind θ^1 C Ori is also ionized by the ultraviolet photons falling on it but the flow of the ionized gas is obstructed in this direction (i.e., the direction of the neutral cloud) due to the dense material and therefore it flows towards the core region thereby mixing with the gas and is dispersed outwards (towards the observer). This will give rise to different 'flows' and the two components could be the result of such flows. It is possible that stellar winds from OB stars can play a significant role in the dynamics. The observational evidence for this was first reviewed by Pottasch (1969). The fast stellar winds from the Trapezium stars could possibly be interacting with the flow of ionized gas coming from the molecular cloud situated behind the Trapezium and the two components could be the result of these interactions along the line of sight. Or it could be the effect of the interaction of neutral condensations with the ionized gas as suggested by Balick et al (1974). The former explanation seems to be plausible since there is evidence for strong stellar wind from θ^1C Ori with terminal velocity of 1650 km/s (Snow and Morton, 1976), and about 500 km/s from θ^1D Ori (IUE observations).

Figs. 4.9 & 4.10 show the iso-velocity contour maps for the two components. Different features of the nebula are also marked on these figures. The

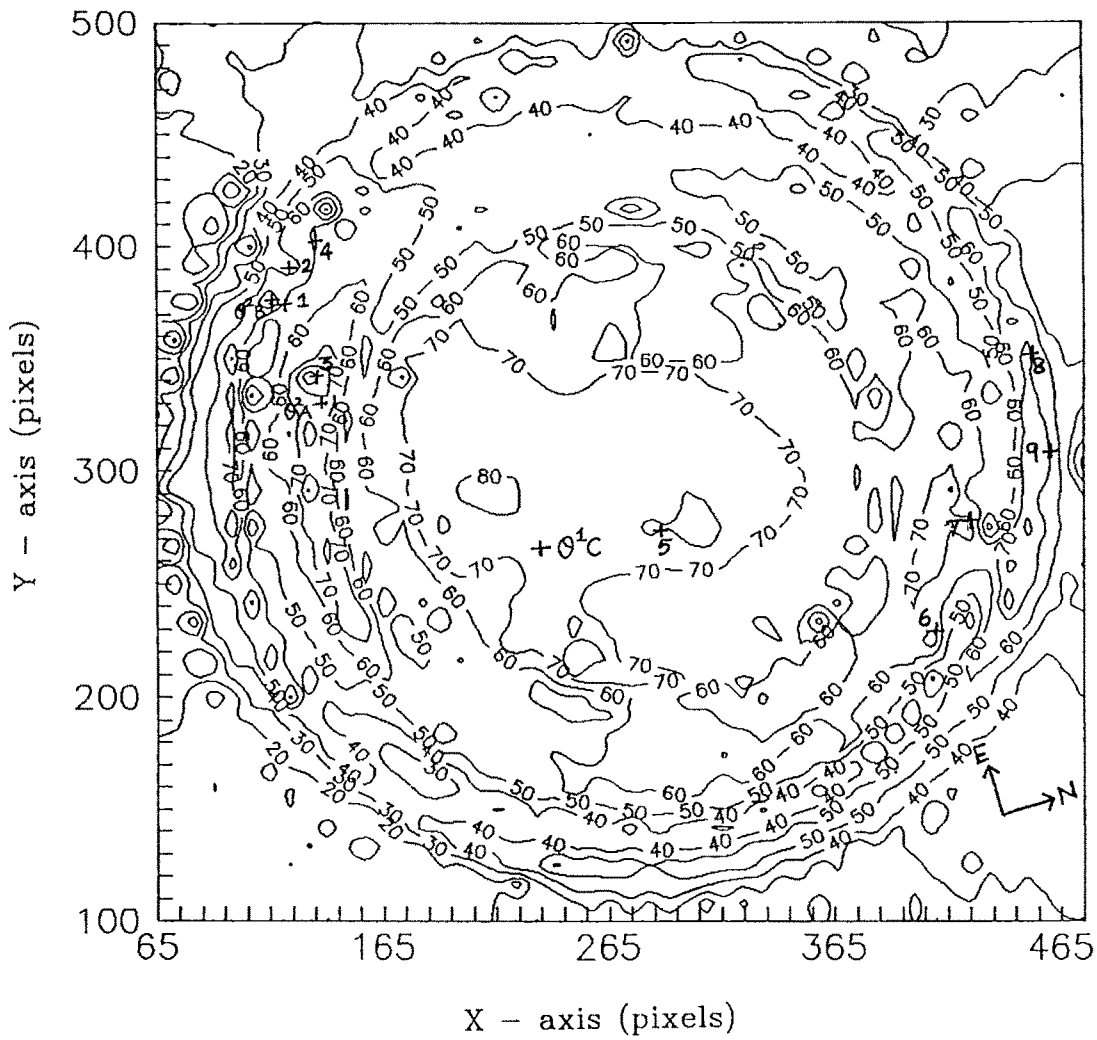

Figure 4.9: Iso-velocity contour map for the narrow component. One pixel corresponds to $\sim 1.23''$ on the sky.

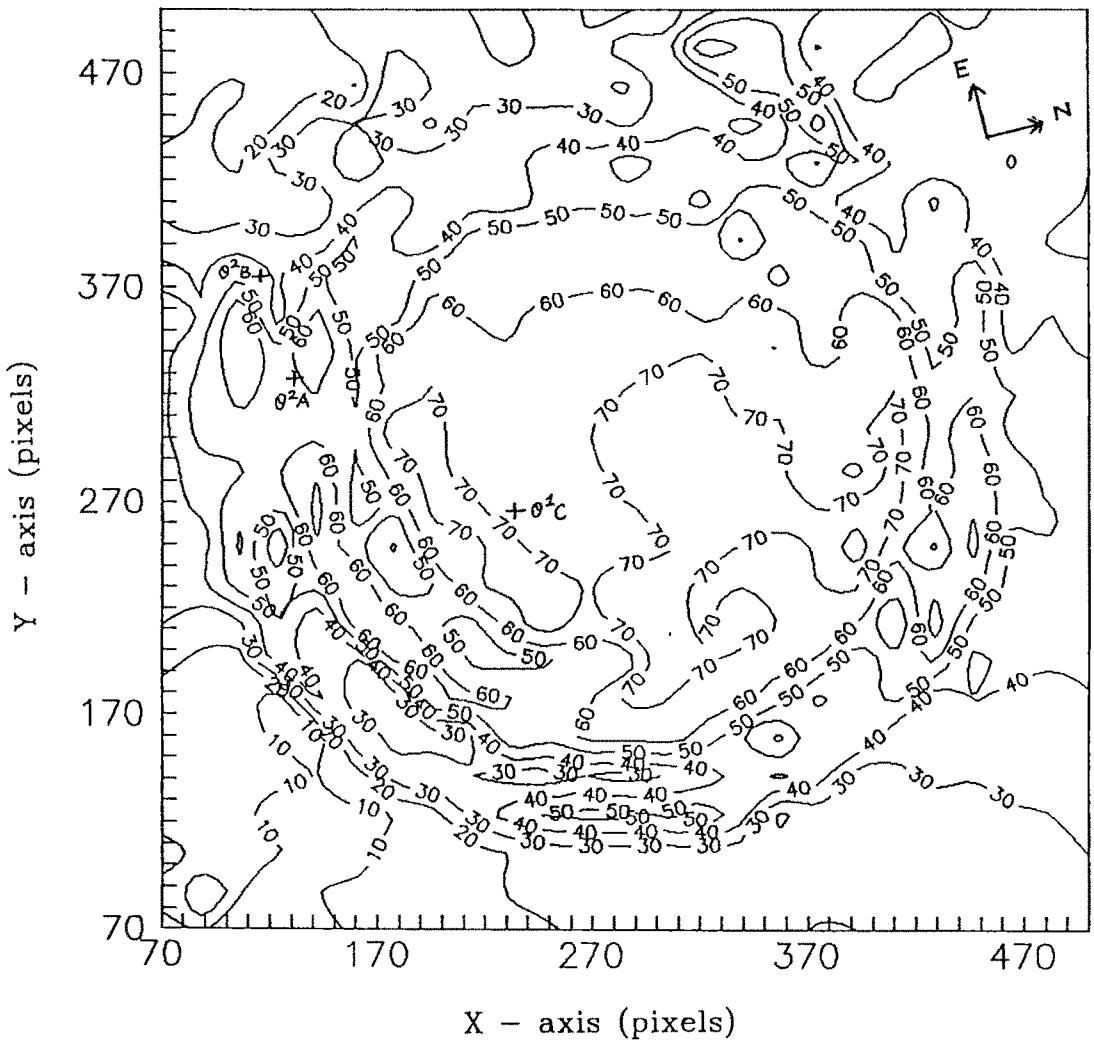

Figure 4.10: Iso-velocity contour map for the broad component. One pixel corresponds to $\sim 1.23''$ on the sky.

iso-velocity contour maps indicate that the general flow is same in both the components except that the velocity field of the narrow component shows certain high velocity flows superimposed on the main flow of the gas. Such flows seem to be absent in the broad component.

Previous studies in Orion gave an indication of line profile asymmetry (Wilson et al, 1959; Smith and Weedman, 1970) and presence of multicomponents in [OIII] 5007 Å line profile (Meaburn, 1984). These studies were followed by Castañeda's (1988) work. His observations were made at higher spectral resolution ($\sim$ 1 km/sec) using a slit spectrograph. He could decompose the profiles into three components having a mean FWHM of (i) 10.02$\pm$ 0.1 km/s, (ii)9.48$\pm$ 0.12 km/s and (iii) 31.26$\pm$ 0.21 km/s. Probably, the narrow component in our study ($FWHM$ $\sim$20 km/s) is the sum of the first two components observed in Castañeda's work which could not be resolved in our observations due perhaps to the lack of adequate spectral resolution. It can be shown, with the assumption that all the components are gaussians and an instrumental FWHM of 6 km/s, that

$$\begin{aligned}(FWHM)_{total} &= [(FWHM)^2_{comp1} + (FWHM)^2_{comp2} + (FWHM)^2_{Ins}]^{1/2} \\ &= (10^2 + 9.5^2 + 6^2)^{1/2} \\ &= 16km/s \qquad (4.1)\end{aligned}$$

which is in good agreement with the narrow component in our work.

4.4.3 Champagne flow

An examination of the contour map of the component one as shown in Fig. 4.9 indicates that the general velocity flow is blue shifted with respect to the Trapezium stars with a decrease in relative radial velocities outwards (114 km/sec/pc). Therefore, the flow seems to be directed towards the observer in accordance with the champagne model (discussed in section 1.12.3), which simply shows that the ionized material from the hot stars in the nebula situated at an edge of the parent molecular cloud is rushing into the interstellar medium due to the pressure gradient established at the HI-HII interface. This 'flow' which is directed towards the observer is termed as the *main flow* (Balick, 1980) or *champagne flow*. This result is in general agreement with those of the earlier authors (e.g., Castañeda, 1988).

4.4.4 Model Profile

In this section, we describe the model emission line profile constructed for Orion near θ^1 Ori complex and compare it with the observed profile at that position. This is to provide a check on the assumptions made regarding the physical conditions in the nebula as well as to see if champagne flow could produce the observed profiles. As far as we know, this is the first attempt to model the observed velocities assuming a champagne flow in the Orion nebula.

Method

The observed line profile results from the integration along the line of sight of radiation emitted by gas moving with different expansion velocities. The line of sight velocity is the sum total of the effects of (i)thermal broadening represented by the Maxwellian distribution of ion velocities (ii) velocity gradient with respect to the radial distance and (iii)turbulent motions. But it is difficult to delineate these effects. It is, however, possible to generate synthetic profiles by putting in reasonable values representing these effects and compare with the observed profiles. The final synthetic profile is obtained under the following assumptions: (i) Champagne flow is assumed where the flow is directed towards the observer, (ii)the distribution of turbulent flow is assumed to be gaussian in nature, and (iii)a constant temperature is assumed throughout the nebula. Therefore, the intensity of emission for a particular line of sight is given (Osterbrock, 1974) as,

$$I(v) = I_o \int_{-\infty}^{\infty} n_e^2 \, e^{-\left[\frac{[v-v(r)]^2}{(2kT/m)+v_T^2}\right]} dv \tag{4.2}$$

where I_o is a constant, k is the Boltzmann constant, m is the mass of the ion, v_T the most probable turbulent velocity and n_e is the electron density assumed constant within the HII region. Actually, eqn. 4.2 becomes a triple integral in r, θ and ϕ, where, r represents the radial distance from the central star to any point in the nebula and θ is the angle that the direct line of sight from the central star to the observer makes with the radius vector r and ϕ is the aperture or field of view from the observer. A schematic of the assumed

geometry for the HII region is given in Fig. 4.11.

The final synthetic profile is obtained by evaluating the triple integral and convolving with the instrument profile $G(v)$ as follows,

$$I(v) = \int_{-\infty}^{\infty} G(v' - v) I(v') dv' \tag{4.3}$$

A line profile is generated using this method for [OIII] line 5007 Å at a position corresponding to about 2 arc minutes from θ^1 C Ori with position angle of 346° and a view angle of 4 arc sec corresponding to our spatial resolution. The velocity gradient due to the champagne flow was taken to be 1.73 km/s/pc (from theoretical work, Yorke et al, 1983) and a temperature of $10^{4°}$ K was assumed. The most probable turbulent velocity was assumed to be 9 km/s. This is in agreement with Castañeda's (1988) value for his first component. The model considers the champagne flow and therefore the profile is obtained by integrating the line of sight velocities coming towards the observer with very little contribution of velocities from the back of the Trapezium. The theoretical profile so obtained is compared with the observed one as shown in Fig. 4.12.

Discussion

The profile seems to match reasonably well with the narrow component of our observed profile. It also matches with the first component of Castañeda's (1988). The second component of Castañeda's can still be accomodated

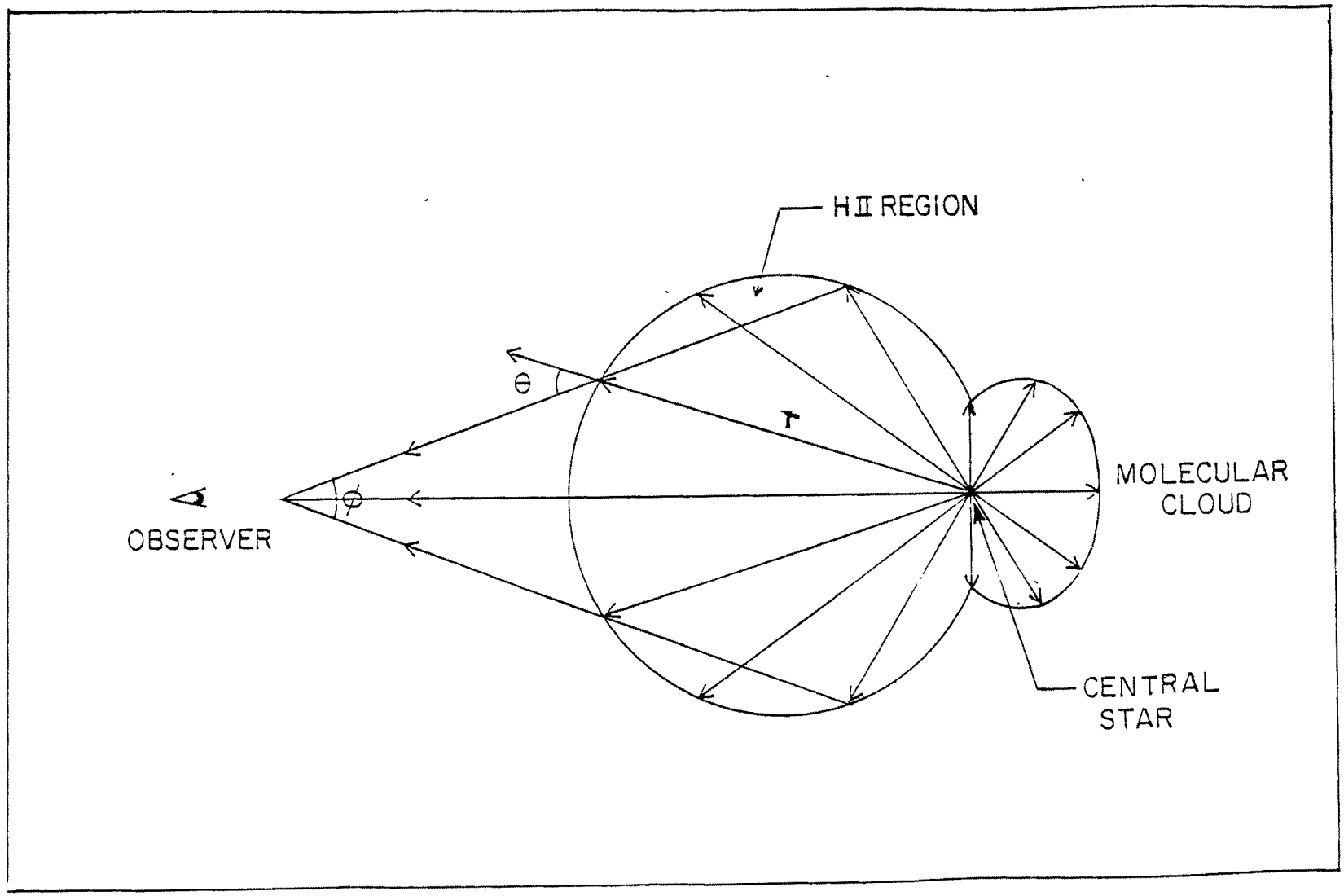

Figure 4.11: Schematic of the assumed geometry for the model profile.

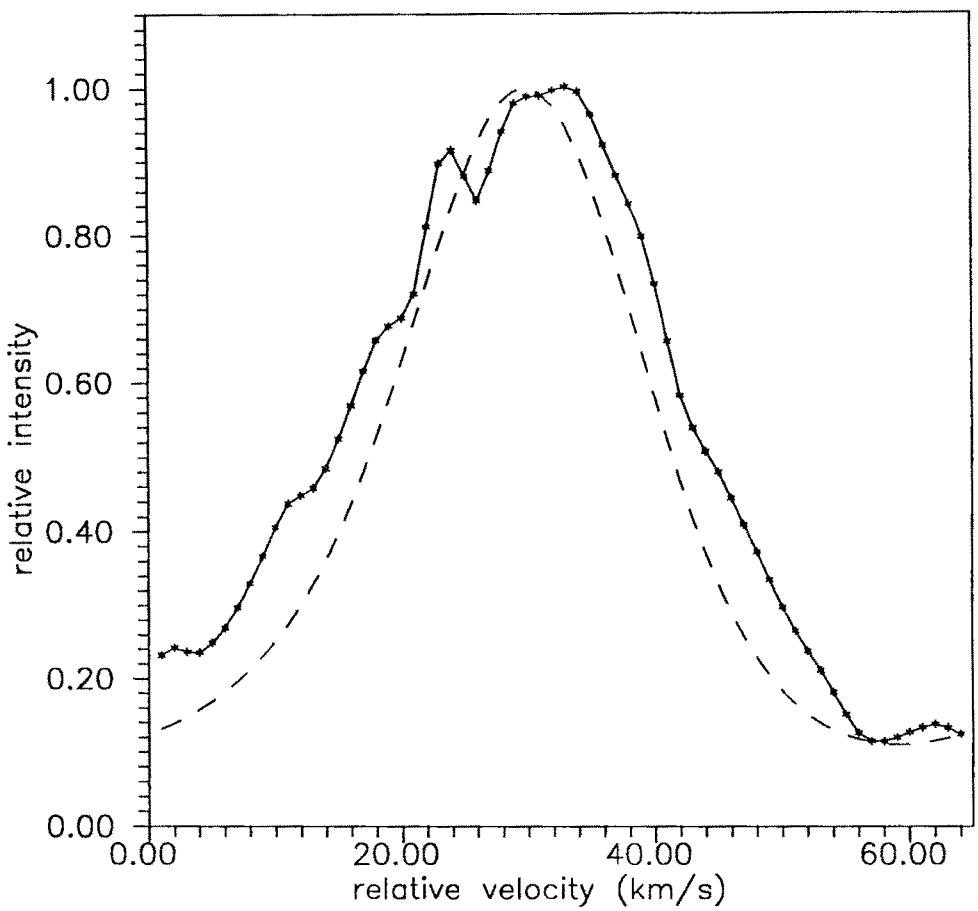

Figure 4.12: Model profile compared with observed profile in [OIII] 5007 Å line in Orion nebula at about 2′ from θ^1 Ori at a position angle of 346°.

within the accuracy of our results.

As far as the second and broader component is concerned, attributing it to the thermal width alone leads to unduly large temperature and it is difficult to defend it. Alternatively it can be explained by either a large velocity gradient or large scale turbulent flows or both; but, that seems to be improbable. Thus the broader component can be attributed to the interaction of stellar wind with the general flow of the gas. In any case, the champagne flow representing the HII region associated with θ^1 Ori seems unrelated to the broader component.

4.4.5 Axisymmetry

From the Fig. 4.9 it is quite apparent that there is a degree of axi-symmetry in the iso-velocity contours centred about 71″ NE of θ^1C Ori. Some type of symmetry is also reported by Hanel (1986) in the iso-velocity map of [OIII] line, which he finds is not observed in the contour maps of other lines ([NII], $H\alpha$, [SII]). Castañeda's study showed elliptical iso-velocity contours centred about the maxima 7″ NE of θ^1 C Ori. This maxima around θ^1 C Ori could not be located in our map due to lack of data in this region. This symmetry, in general, can be expected in an HII region powered by a single star. From this also it is probably clear that the main ionizing star for the central HII region in Orion is $\theta^1 C$ Ori.

4.4.6 Velocity flow around θ^2 Ori

The HII region around θ^2 Ori is supposed to be physically separate and unconnected from the main HII region around Trapezium (Peimbert, 1982). Some of the studies which favour this argument are: (i) the spectroscopic studies in [NII] line of Orion show that the radial velocities were found to be different around θ^2 Ori when compared to θ^1 Ori (Deharveng, 1973); (ii) the optical linear polarization map due to Pallister et al (1977) shows a centrosymmetric pattern due to the scattering of stellar light by the nebular matter, around the Trapezium (θ^1 Ori) as well as θ^2 Ori. It is observed further that the pattern in the region around θ^2 Ori, is unconnected to that around θ^1 Ori (Pallister etal, 1977); (iii) in the chemical abundance study it is found that the ratio of He^o/He^+ is large in the direction of θ^2 Ori when compared to θ^1 Ori. This implies that there is a lower degree of ionization in the direction of θ^2 A Ori compared to that in the direction of θ^1C Ori indicating that the radiation fields of θ^1C Ori and θ^2 Ori are uncoupled . Also, lack of dust and CO emission to the south-east of the bar and lower extinction in the direction of θ^2A Ori than towards θ^1C Ori suggest that θ^2A Ori is a foreground object relative to the Trapezium stars (Peimbert, 1977). Therefore it was necessary to study the velocity field around θ^2Ori separately.

That the velocity fields around θ^1 and θ^2 Ori are unconnected can be seen from our observations presented as the contour maps in Fig. 4.9, and

Fig. 4.10. Our velocity map showed that there are certain high velocity regions around the stars θ^2 A Ori and θ^2 B Ori (discussed in the following section) but there is no particular well defined velocity pattern around these stars. The interaction of the flow from the HII region associated with θ^1 Ori with that from the HII region associated with θ^2 Ori might have caused a complete disruption of the pattern : the redward components of the θ^2 Ori HII region getting partially or fully cancelled by the blueward components of the flow from θ^1 Ori. This can happen as the two opposing flows cannot seep through each other because the ion mean free path is much smaller than the size of the HII region.

HII region around θ^2 B Ori

A region of particular interest is found in the [OIII]/$H\beta$ map due to Pogge et al (1992), south-east of the bar ionization front centred roughly on the star θ^2 B Ori, where there is a sudden drop in the mean value of [OIII]/Hβ ratio to 1.3 and then a distinct increase to 2.3 about 10″ south-west of θ^2A Ori. It was interpreted to be a region which is being shadowed from the θ^1 C Ori due to the dense absorbing material around the bar. The intensity ratio maps of Pogge et al (1992) show further that the ratios [NII]/$H\alpha$ and [SII]/$H\alpha$ are higher in the region centred on θ^2 Ori. The optical depth map of these authors shows that the extinction is not particularly lower compared to the surrounding regions. This probably suggests that the region has emission particularly from low excitation ions indicative of a weaker

radiation field around θ^2 B Ori, a B0.5 type star (Table 4.1) than that around the Trapezium. Further and more importantly our velocity map shows a velocity field structure different and delinked from that surrounding $\theta^1 C$ Ori. This is also supported by the polarization map (Pallister et al, 1977), where it is found that the centro-symmetric pattern around θ^2 B Ori is unconnected with that of θ^1 C Ori. In view of this we propose an alternative explanation that the region centred on $\theta^2 B$ Ori is actually its associated HII region.

4.4.7 The Orion dark bay

The dark bay feature is located east of the Trapezium stars and at the north edge of the bar ionization front. It is found to be a region of low surface brightness and hence is associated with low emission. It has been verified that the dark bay feature is not a manifestation of the effect of heavy extinction with the help of the radio continuum map at 21 cm (Van der Werf & Goss, 1989), the CO map (Thronson et al, 1986), [CII] 157.7 μm map (Stacey et al, 1992) and the optical extinction map (Pogge et al, 1992). Our results on this region show relatively low velocities ($\sim$ 20-30 km/s) compared to the θ^1 Ori HII region. The low velocities actually suggest an obstructing material to the expanding gas in the HII region.

Table 4.2: High velocity positions with reference to θ^1 Ori

Sl. No.	Position from Trapezium stars (arc minutes)		Relative velocity (km/s)
1.	2.30 S	2.29 E	65
2.	2.20 S	2.60 E	67
3.	2.05 S	1.60 E	53
4.	2.05 S	2.85 E	57
5.	1.20 N	0.05 W	51
6.	3.60 N	0.78 W	50
7.	3.96 N	0.25 W	59
8.	4.60 N	1.80 W	53
9.	4.70 N	0.80 W	69

4.5 High Velocity Flows

Certain localized regions of high velocities (~50 km/s) are found on the iso-velocity map (Fig. 4.9). Some of these regions correspond to identified stellar sources and some others do not. The positions given in Table. 4.2 have a positional accuracy of $\sim$ 4 arc sec. These regions are of the size of a few arc seconds. The table also lists the relative radial velocities. It can be seen that the radial velocities are red-shifted with respect to the general flow, in all the cases. In what follows, we discuss these in detail.

4.5.1 Around identified stellar sources

(i) $\theta^1 C$ Ori and (ii) $\theta^2 B$ Ori. The reason for high velocity around θ^1 C Ori is that the champagne flow is directed towards the observer and hence the flow velocity is maximum around the star and decreases away from it. Further acceleration is possible through other mechanisms, especially by radiation pressure.

Radiation Pressure

When the radiation from a hot star is absorbed by the surrounding dust, it gets heated up and the energy is radiated isotropically in the infrared. The photons carry momentum with them along with the energy. Therefore, when the radiation is absorbed by the dust, the momentum also gets transferred to the dust since the photoabsorption crossection for the dust is larger than that for ions. This results in a force on the dust, which is much greater than the inward force due to gravity, and the dust is rapidly accelerated outwards. The radiation force on the dust particle is given as follows (Osterbrock, 1974):

$$F_{rad} = \pi a^2 \int_0^\infty \frac{L_\nu}{4\pi r^2 c} P_\nu \, d\nu \sim \frac{a^2 L}{4r^2 c}$$

where P_ν is the efficiency of the particle for radiation pressure, a is the size of the dust particle, L_ν is the luminosity of the star per unit frequncy interval, L, the total luminosity, and r is the distance from the star. The collisions between the dust and the gas will then accelerate the gas outwards

resulting in high velocity flow. Furthermore, there are observations in the optical and infra-red regions showing that there is an anomalous extinction in Orion nebula ($A_v/E(B-V) \sim 5.0$) compared to other diffuse clouds ($A_v/E(B-V) \sim 3.0$)(Johnson, 1968). This anomalous behavior is accounted for by the presence of large dust grains ($\sim 0.1\mu m$) around $\theta^1 C$ Ori (Sorell, 1992). Also, the optical depth $\tau(H\alpha)$ map due to dust derived from the $H\alpha/H\beta$ Balmer decrement by Pogge et al (1992) shows that the reddening of stars in the foreground of Orion is small (E(B-V) = 0.05 mag, Breger et al, 1981), while the reddening toward $\theta^1 C$ Ori is E(B-V) =0.32 mag (Bohlin & Savage, 1981), thus, it was pointed out that most of the additional extinction should arise in the nebula proper. This indicates the presence of large amount of dust around θ^1 C Ori. Therefore, the high velocity flows near the hot stars found in our observations could be partly caused by radiation pressure-driven stellar winds.

4.5.2 Around protostellar sources

Shock excitation

An indication of high velocity flow with a velocity jump of $\sim$ 50 km/s (refer Table 4.2, position 5) around 1.2 arc min NW of Trapezium stars is found to be corresponding to a peak of shocked H_2 emission observed in $2.12\mu m$(Beckwith, 1978, Peak I). Shock excitation of the H_2 was first sug-

gested by Gautier et al (1976) and Kwan and Scoville (1976) to explain the H_2 emission. Several model calculations were made in order to check this possibility (Hollenbach and Shull, 1977; London et al, 1977; Kwan, 1977). The model calculations gave limits to the shock velocities and volume densities. With these values of density and velocity, the minimum pressure required to drive a shock was given as $\sim 3 \times 10^{-7}$ dynes cm^{-2}. Since there was no observed luminosity source which could drive such a shock continuously by applying the required pressure on the molecular cloud, the shock excitation of H_2 was attributed as due to an energetic explosion such as that from a supernova (Beckwith etal, 1976). A feature corresponding to this peak (position 5 in Table 4.2) was also observed in the HST image as a prominent dark cloud followed by a 20″ jet-like feature apparently emanating from a star located at the edge of this cloud (Hester et al, 1991). A corresponding feature was also reported in the [SII] line at this position (Raju et al, 1993).

A jet like feature

There is an interesting feature in the form of a knot like structure observed in the image about 1.5 arc min north west of the Trapezium stars(Fig 4.2). It is found to have a radial velocity of about -11 km/s with respect to the surrounding region and the line profile shows a FWHM of about 90 km/s (Fig 4.13) and there is a split in the line profile showing an expansion velocity of 12 km/s. There is no report of such a feature in the earlier studies in that position. This could possibly be the effect of stellar winds from Trapezium

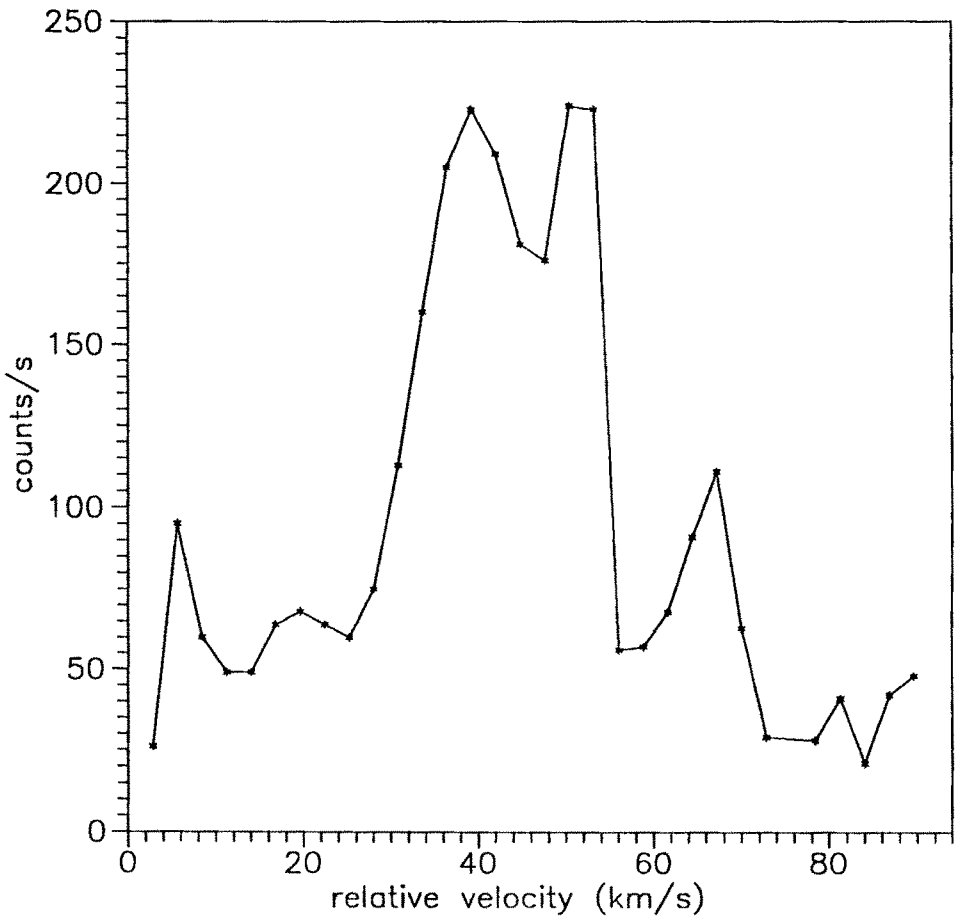

Figure 4.13: A line profile at the jet like feature about 2.3 arc min NW of Trapezium.

ablating a neutral blob. The blob eventually becomes partially ionized due to stellar photon flux or shock compression. These are called partially ionized globules (PIG). PIGs are small dense neutral globules completely covered with ionization fronts with the ionized gas expanding into the low density medium (Dyson, 1968a,b, Kahn 1964). Evidence for the existence of PIGs was found by Dopita et al (1974). The effect of stellar wind on these globules was first modelled by Dyson (1975). The large FWHM found by us also possibly suggests the stellar wind interaction.

Due to the sky projection effect, the exact position of the globule from the central star is difficult to be known, therefore, two possibilities could be considered in order to explain the feature (i) The globule is considered to be situated near the hot star (L=10^{38}ergs/sec). In this case, the velocity observed (-11 km/s) is not the actual velocity but could be the projected velocity along the line of sight (i.e., $v_{actual} = v_{proj}$ /cosθ, θ being the projection angle). In this case, however, ionization effects due to shock (stellar wind) should be seen. We do not find enhanced [OIII]/Hβ (from Pogge et al, 1992) in this region implying less possibility for the globule to exist in the proximity of θ^1 C Ori. (ii)The globule is situated rather far away from the star with the observed velocity being the actual one without much of projection effect. This situation can be explained by considering Dyson's model (1975). He considered the case where the globule is supposed to be situated at a distance of 1 pc from the star and the rate of mass loss from the star is assumed to be $10^{-6} M_{\odot}$/yr. Then the velocities of the shocked structures are

found to be about 10 km/s implying that there is no significant kinematic or ionizing effect of stellar winds on the globule in such a case. The blue-shift in the Doppler velocity indicates that the globule is situated in front of the Trapezium stars.

4.5.3 The molecular cloud region

According to the Blister model (Zuckerman, 1973) , the HII region in Orion is in front of and eating into the molecular cloud behind. The molecular line studies of ^{13}CO (Bally et al, 1991) have shown that the structure of molecular cloud is highly filamentary. The $BN - KL$ (Becklin-Neugebauer-Kleinmann-Low) infrared nebula is found to be the young star forming region located in front of the OMC-1 about $0.1 - 0.2$ pc behind θ^1C Ori. The ultraviolet photons from the Trapezium stars penetrate the molecular cloud and photodissociate the molecules (mainly molecular hydrogen and CO) and photoionize the atoms (carbon and silicon).

Studies in the past showed that the photodissociation regions (regions that are situated outside the HII regions where the molecular hydrogen undergoes photodissociation) exhibit CO rotational lines in millimeter, submillimeter, far-infrared regions as well as CII, [OI] and CI optical lines. The existence of photodissociation region was first unveiled in the optical lines of CI and [OI] (Munch and Taylor, 1971; Hippelein & Munch, 1978; Munch and Hippelein, 1982) and in the radio recombination lines of carbon (Palmer et

al, 1967). Certain high velocity flows are found in our observations overlying the molecular cloud (Positions, 6,7,8 and 9 in Table 4.2). These flows are not associated with any peculiar features (Knots or HH objects) detected earlier (except position 5). The possibility is that there could be an infrared source embedded in the cloud, where star formation is being just initiated by a shock such as a supernova explosion. The hot spots found in the radio ^{12}CO map (Loren, 1979) and other ^{13}CO features (Sugitani, 1986 and references therein) do not correspond to any of these features and hence these must be new sources. Alternatively, this can be explained in terms of partially ionized globules (PIGs). The heliocentric radial velocities of the Trapezium stars (29 km/s) and the molecules embedded in the core of PIGs (26 km/s) suggest that the Trapezium and the PIGs are formed from the same neutral cloud into which the ionization front from θ^1 C Ori is eating into. The model presented by Dopita et al (1974) show that PIGs are formed near to the front and are also moving into the molecular cloud, thus explaining the red-shifted velocities found by us.

4.6 The bar ionization front

The bar represents the ionization front region formed at the HI-HII interface. It serves as a laboratory provided for studying the interaction of the ionized material with the neutral cloud. It is supposed to be situated at about 1.5 arc minutes south-east of the $\theta^1 C$ Ori extending from $\alpha = 5^h 32^m 51^s$ and $\delta =$

$-5^o27'30''$ to $\alpha = 5^h33^m03^s$ and $\delta = -5^o25'36''$ (Elliot and Meaburn, 1974) and going into the background molecular cloud away from the observer. The optical, radio and infrared observations indicate that the bar is seen almost edge-on (Zuckerman, 1973; Balick et al, 1974). The bar ionization front as observed in the recent images obtained from the Hubble space telescope (Fig. 4.14 as reproduced from O'Dell, 1992) indicates that it is originating from the Trapezium stars and not from θ^2 Ori. This is because the front is slightly but clearly concave towards the side of the Trapezium complex and there is diffuse matter in between the Trapezium and the ionization front with a sharp gradient in density towards the convex side (i.e., the side facing θ^2 Ori).

The Orion bar has been studied extensively in the near infrared continuum (Becklin et al, 1976), far infrared continuum (Werner, 1976; Fazio et al, 1974), near infrared line emission (Hayashi et al, 1985), interstellar infrared emission features (Aitken et al, 1979; Geballe et al, 1989; Roche et al, 1989; Bregman et al, 1989), molecular lines (Omodaka et al, 1987) and in $3.3\mu m$ emission (Sellgren et al, 1990). It was first suggested by Fazio (1974*b*) and Balick (1974) that the infrared emission may be associated with the ionization front. Later, observations at 2 and 10 μm (Becklin et al, 1976) confirmed the existence of the bar. The infrared emission was interpreted to be due to the heated dust near the ionization front. It was also shown (Becklin et al, 1976) that the luminosity sources responsible for this emission were the Trapezium stars.

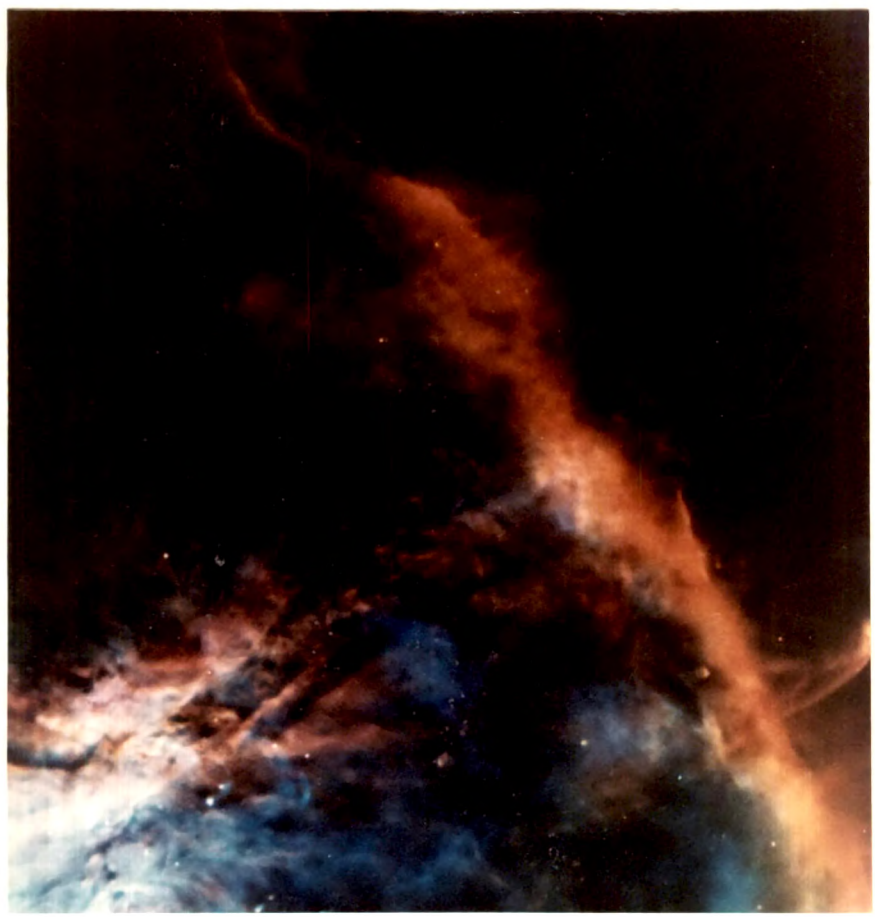

Figure 4.14: The ionization bar front as revealed by the wide field camera images obtained by the HST (from O'Dell et al, 1993).

4.6.1 Velocity field around the bar ionization front

We have mapped the velocity field near the 'bar' ionization front in the [OIII] 5007 Å line (Fig. 4.9). There seem to be certain localised positions around the bar of the size of a few arc secs where there is a rise in velocity of about 30-40 km/s compared to the surrounding regions. But there is no well defined continuous increase in velocity all along the bar in [OIII] velocity map. This can be explained when we compare our velocity map with the emission-line flux ratio maps of [OIII]/Hβ, [NII]/Hα and [SII]/Hα obtained by Pogge et al (1992). It is clearly seen that the [NII]/Hα and [SII]/Hα maps define the razor sharp feature of the bar. However, in the [OIII]/Hβ map, the structure corresponding to the bar is quite diffused and displaced (it is closer to the star than the bar in [NII] or [SII]) and only certain ionized clumps are prominently seen. It appears that the velocity jumps observed by us in some localised regions around the bar are associated with the clumpy features seen in the [OIII] map by Pogge et al (1992). Also the HST images obtained in different lines [NII], [OIII], $H\alpha$ and [SII] (Hester,1991) corroborate with this.

The ionization structure found around the front is obvious since the ratios [NII]/$H\alpha$ and [SII]/$H\alpha$ are sensitive to the rapid change in the state of ionization across the HI-HII interface, whereas [OIII] emission arises in the fully ionized zone and therefore [OIII]/$H\beta$ ratio tracks the ionization structure within this zone, and emphasizes structures different from those found in [SII] maps.

In the electron density map presented by Pogge et al (1992) from the [SII] doublet ratio, the Orion bar ionization front appears as a density enhancement in which the density increases from 2000 cm^{-3} to 3200 cm^{-3} and then drops outward across the front. In the present work, we have obtained a velocity profile, for the first time, across the bar by taking a scan perpendicular to it as shown in Fig. 4.15. There is a rise in velocity of about 20 km/s at the bar position. The velocity from the direction of θ^1 Ori increases from 45 km/s to about 55 km/s across the bar and then falls back to 35 km/s outwards. A comparison of the velocity profile with the density profile (Pogge et al, 1992) shows that when the density is high, the velocity is relatively low and vice versa. This is in accordance with Rankine-Hugoniot jump conditions for flows across isothermal shock fronts, viz.

$$\rho_1 v_1 = \rho_o v_o$$

where ρ_o, ρ_1 and v_o, v_1 are the densities and velocities behind and in front of the shock front respectively. However, it should be noted that the density found from the [SII] line could be different from that found from [OIII] line as these ions occur at different regions. But the electron density derived from [SII] lines does not show much spatial variation. Furthermore, there seems to be a positional difference between the [SII] bar feature and [OIII] bar feature as can be inferred from Pogge et al (1992). However, the velocity profile across the bar obtained by us is quite broad as is the density profile of Pogge et al (1992).

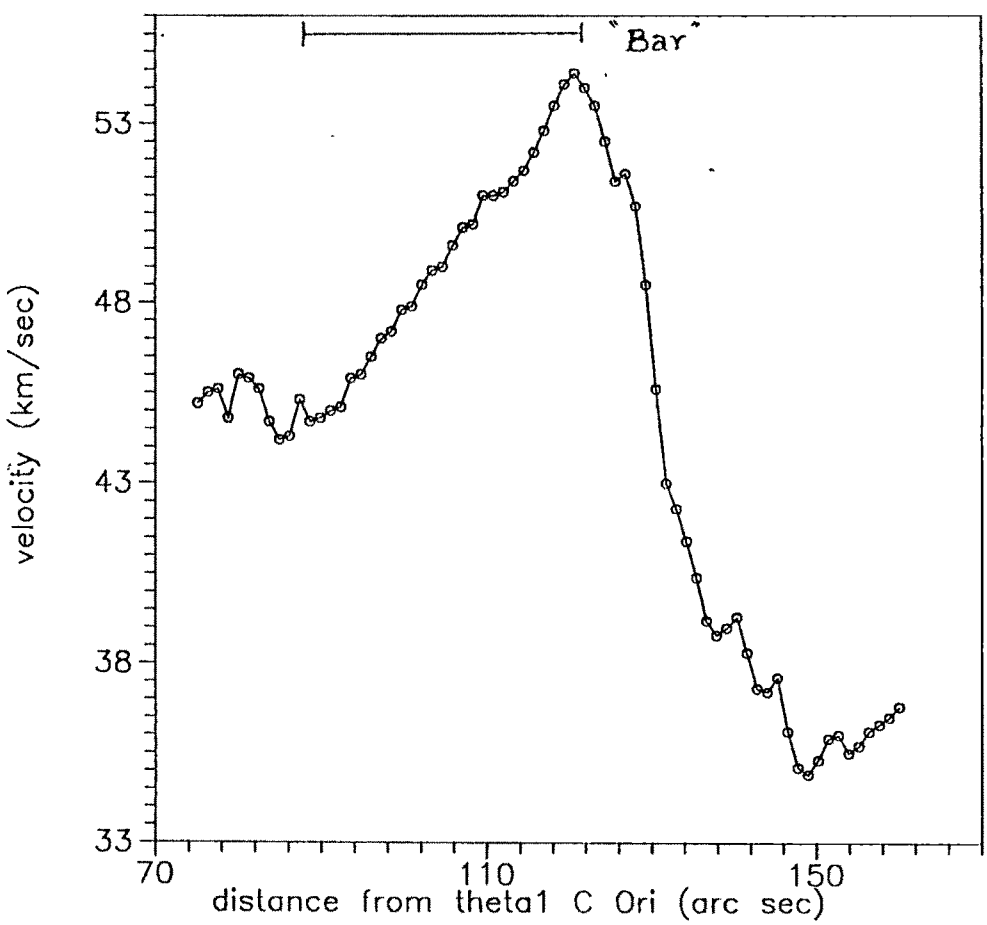

Figure 4.15: Velocity profile across the bar ionization front.

4.6.2 Width of the shock front

As discussed in section 1. 6, a shock wave precedes the expanding ionization front into the neutral cloud because of the supersonically expanding HI-HII interface. Our observations show a velocity jump across the front while the jump in electron density is reported by Pogge et al (1992) in the density profile obtained by them in the optical region and a temperature jump is reported in the CO maps (Loren, 1979). These observations suggest that the shock could most probably be a J type of shock (shock across which discontinuous jump in physical parameters like temperature, density and flow velocity takes place, Hollenbach et al, 1988). Also, there are observations (Johnson, 1983) indicating dissociation of molecules taking place along the shock which again emphasizes on the shock being a J type shock. The width of the shock front in a fully ionized gas is given as follows (Tidmann, 1958)

$$l = (m_H v_s^2/e^2)^2/690 n_e L \tag{4.4}$$

where m_H is the hydrogen mass, e is the electronic charge, v_s is the shock velocity, n_e is the density and L is the coulomb logarithm given as:

$$L = ln[\frac{3}{4(\pi n_e)^{1/2}}(kT/e^2)^{3/2}] \tag{4.5}$$

Taking the temperature in the ionized gas to be 10^4°K and a density of 3200 cm $^{-3}$, L is found to be $\sim$ 24. It is seen from eqn. 4.4 that the width is

Table 4.3: Theoretically calculated parameters of the shock front

angle (degress)	Actual absolute velocity(km/s)	Width of the front in (pc/arcsec)
89	1750	$1.1\times10^{-1}/(48.0)$
88	875	$690\times10^{-3}/(3.0)$
87	583	$1.35\times10^{-3}/(0.6)$
86	438	$4.33\times10^{-4}/(0.19)$
85	350	$1.76\times10^{-4}/(0.079)$

sensitive to shock velocity. We have calculated the actual shock velocity for five different angles (angle that the shock velocity vector makes with the line of sight) assuming that the bar is observed near edge-on (Elliot and Meaburn, 1984). With these values of shock velocities, the width of the shock front is calculated and the results are tabulated in Table. 4.3. The observed projected width is found to be about 35 arc secs from the density profile across the bar from Pogge et al (1992).

4.6.3 Ionization mechanism at the shock front

As discussed in section 1.5, there are basically three mechanisms by which ionization could take place in an HII region: (i) photoionization (ii) collisional ionization due to the compression by a shock wave and (iii) charge-exchange reactions. In order to distinguish between the ionization mechanisms, Baldwin et al (1981) have proposed a classification system based on the strengths

of the emission line ratios (using the available data). However, this method has certain drawbacks as was pointed by Pogge et al (1992) and the shock excited region cannot be isolated from the stellar photoionized region using this method alone, since the regions are all seen overlapping in projection. For example, Pogge et al (1992) have plotted the diagnostic line ratios (like [SII]/Hα vs [OIII]/Hβ) in a shock excited region of the nebula involving HH objects. According to Baldwin et al's (1981) method, it was expected that all these points should lie away from the general locus of HII region-like objects, which was not the case. Pogge et al have interpreted that this could be due to these regions being embedded in a high surface brightness photoionized nebula and therefore could not be decoupled easily with their data and it was concluded that, since HH objects are kinematically distinct with velocities more than 60 km/s (Canto et al, 1980), it should be possible to make the distinction between shock ionized and photoionized regions from kinematic studies.

Models of ionization fronts were generated by Mallik (1977) and it was shown that the temperature near the front can reach high values, resulting in an enhancement of the collisionally excited lines when compared to less temperature-sensitive hydrogen recombination lines. The signature of shock in an ionized gas is supposed to be a combination of a hot collisionally ionized region, with high values of [OIII] 4363/[OIII] (4959+5007) and a low excitation photoionized recombination region characterized by strong [OI] and [SII] lines (McKee, 1987). The shock emission spectra modelled by Shull et al

(as referred to in McKee, 1987) shows that the ratio [OIII] (4959+5007)/Hβ peaks (324) at a shock velocity of 130 km/s whereas the ratio [OI] 6300/Hβ and [SII]/Hβ peak (685 & 1200 respectively) at 30 km/s. Therefore by measuring the abundances of these ratios it should be possible to say whether the gas is collisionally ionized or photoionized.

The velocity (actual) around the bar ionization front is inferred to be more than 100 km/s from our observations (Table 4.3) considering that the front is making an angle nearly 85° with the line of sight.

On the basis of this we suggest that the O^{++} could have been produced by shock ionization, atleast, in part.

A schematic model for the Orion nebula

Based on the foregoing discussion of the results of the velocity field obtained by us and the other results, we present a schematic model for the structure of the Orion nebula shown in Fig. 4.16.

4.7 Turbulence

The third aspect of our studies on the velocity field structure in Orion involves charecterization of turbulent motions. As has been mentioned earlier, the presence of random fluctuations in radial velocities and the abnormal widths

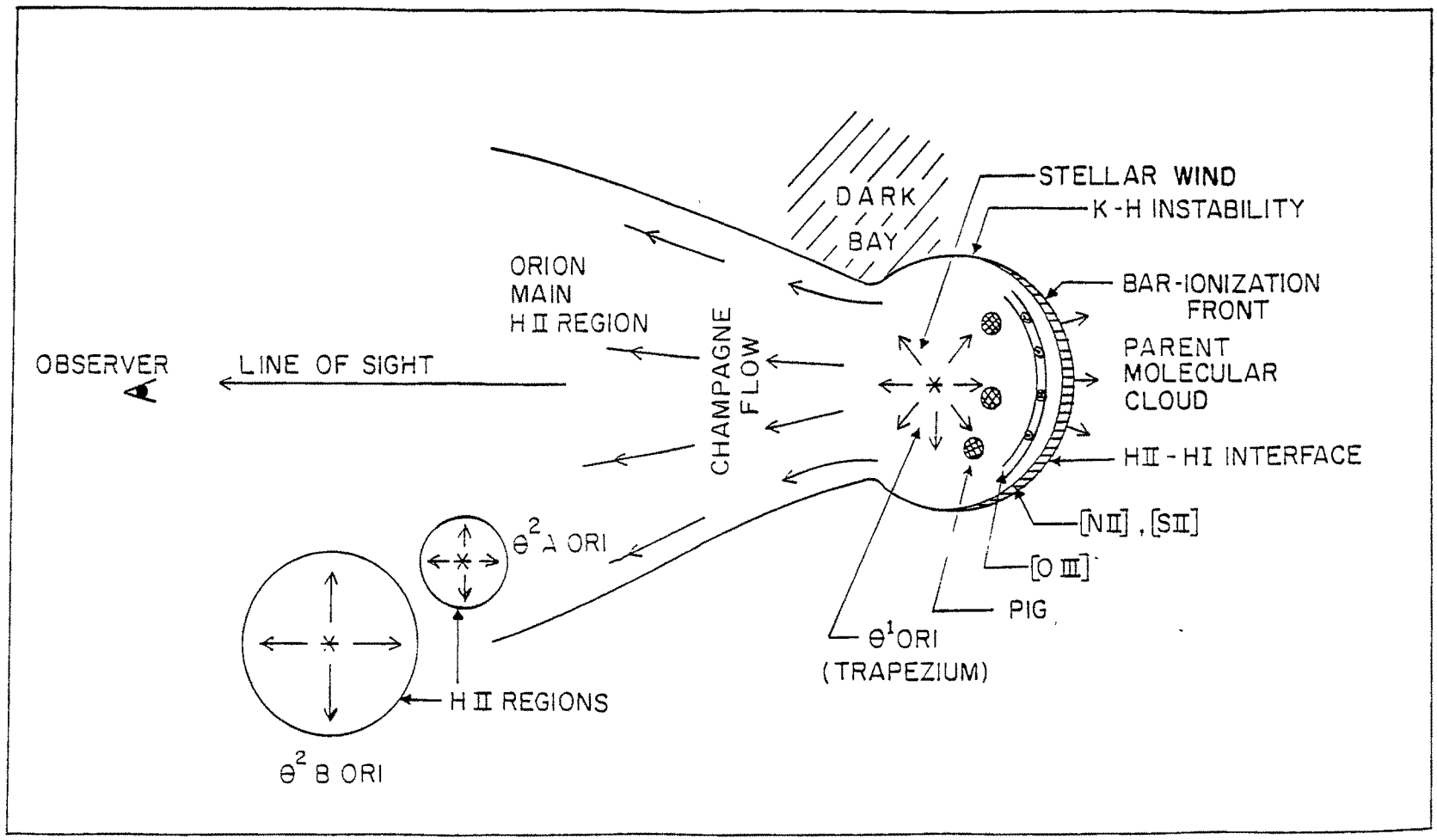

Figure 4.16: A schematic model for the Orion nebula based on the velocity field structure.

of emission lines has been established in the literature. The random motions in the fluid actually characterize the statistical order in the flow. Therefore, in order to study the random components we have made a statistical analysis from the large number of data points. Our study includes the analyses of the following: (i) Distribution of relative velocities and (ii)two point correlation function such as the Structure function.

4.7.1 Distribution of radial velocities

Turbulence being a stationary random phenomena, the distribution of radial velocity components, corrected for systematic flows, is assumed to follow a gaussian. In our data, we do not get absolute values of radial velocities but only the relative values. However, this would not matter as it would only change the 'dc' component. Therefore, histograms of relative radial velocities (uncorrected for systematic flows) in a window size of 4 arc sec against the number of points are generated and are shown in Figs. 4.17, 4.18 for the two components. One can see that the distribution follows fairly well a gaussian in the case of both the components. This probably shows that the random component of the radial velocities follows a gaussian distribution as assumed in the Kolmogorov theory. Our results are in corroboration with those of Castañeda's (1988). Since the distribution shows a gaussian nature even without accounting for the systematic mass flow, we may conclude that the effect of the latter is not very significant, atleast, in the present case.

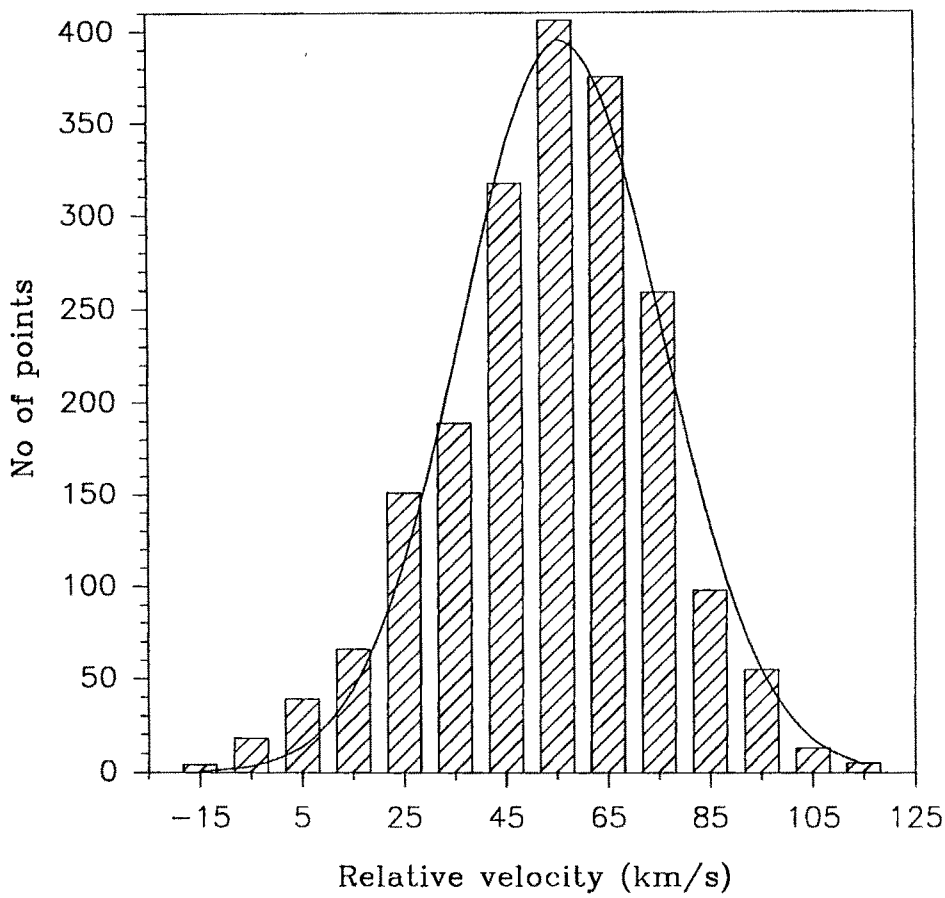

Figure 4.17: Histogram showing the velocity distribution for narrow component over the entire region of observations on Orion. The window size is 4 arc sec.

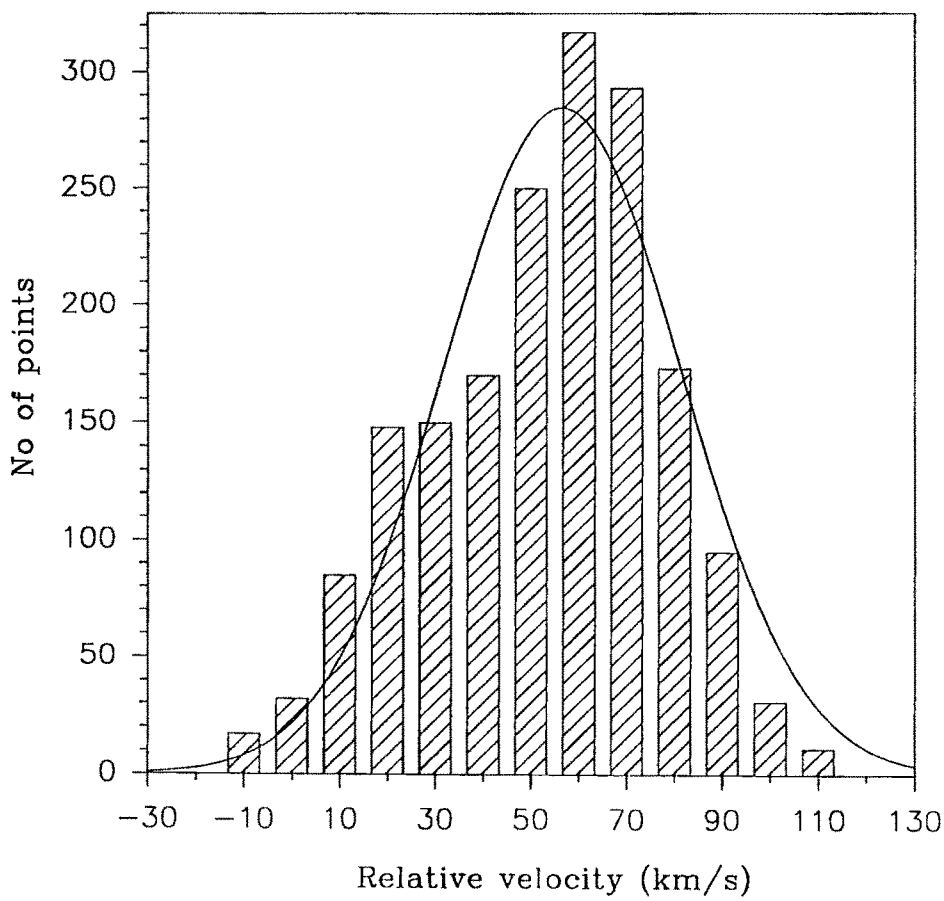

Figure 4.18: Histogram showing the velocity distribution for broad component over the entire region of observations on Orion. The window size is 4 arc sec.

4.7.2 Structure function

The averages and correlations of different physical quantities give a better way of understanding the behaviour of the fluid pattern (Scalo, 1984). The structure function is defined in order to make the statistical studies under the assumptions that the fluid is (i) isotropic, (ii) homogeneous and (iii) incompressible i.e., the density is constant (Kaplan, 1966) and free from any discontinuities like shock fronts etc. It is given by,

$$B(r) = < |v(r') - v(r'')|^2 >$$

where $r = r' - r''$ is the scale under investigation for velocity correlation and $v(r')$ and $v(r'')$ are the measured radial velocities at the points r' and r'', . This method was first used by von Hoerner (1951) and later, applied by Courtes(1955), Munch (1958), Louise and Monnet (1970), Scalo (1984), Roy and Joncas (1985), and very recently by Castañeda (1988) and O'Dell et al (1993). It was pointed out by Scalo (1984) that the structure function was a more appropriate method of analyzing the velocity fluctuations in HII regions, since it can characterize the correlation even in the presence of large scale spatial gradients. Since the calculation of the structure function involves the difference of velocity at two points, any number of points can be used to evaluate the function at a given distance which offers greater statistical accuracy. Its large absolute value makes it less sensitive to instrumental dispersion corrections (Castañeda, 1988). According to the standard model of Kolmogorov, $B(r) \propto r^{2/3}$. Therefore, the study of turbulence in gaseous

nebulae is reduced to the study of spatial fluctuations in the mean radial velocity along the line-of-sight. The structure function was computed by selecting all the possible combinations of pairs of points for the different sample sizes: $30'', 50'', 120'', 140'', 160''$. The minimum scale size was 4 arc sec as permitted by our spatial resolution. The structure function was evaluated in certain regions of interest which are discussed here.

Around θ^1 C Ori

The structure function was first evaluated in about 2 arc min area around θ^1 C Ori. Since the region selected is small, the conditions of the fluid being homogeneous and isotropic are likely to be satisfied as required by the Kolmogorov's theory. Any discontinuities and large scale gradients (such as that due to champagne flow) in velocities are subtracted from the radial velocities. A least square fit for the function representing a power law $B(r) = cr^n$ gives the value of the exponent $n = 0.998$ with correlation coefficient $=$ 0.978 for the first (narrow) velocity component (Fig. 4.19), for scale size of upto $100''$. The second (broad) velocity component also showed a similar behavior with $n = 1.23$ and correlation coefficient =0.97 (Fig. 4.20), for scale size of upto $100''$. Thus, the slope is found to be much larger than Kolmogorov's predictions. Around 120 arc sec from the Trapezium stars there is a sudden fall in the structure function. This hook is observed in all the earlier studies made on the nebulae. It seems to be the effect of the decrease in the number of points at larger separation and hence could be an

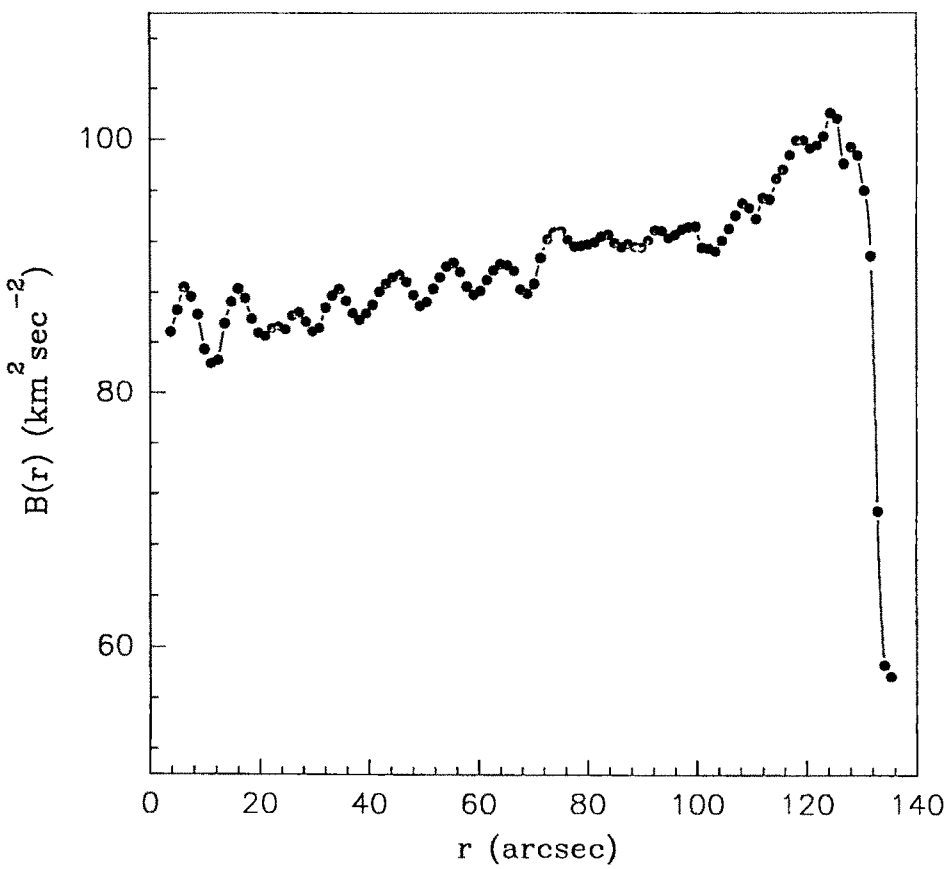

Figure 4.19: Structure function around 2 arc min of θ^1 C Ori for narrow component. The standard deviation in each data point corresponds to $\sim \pm 12$ km/s.

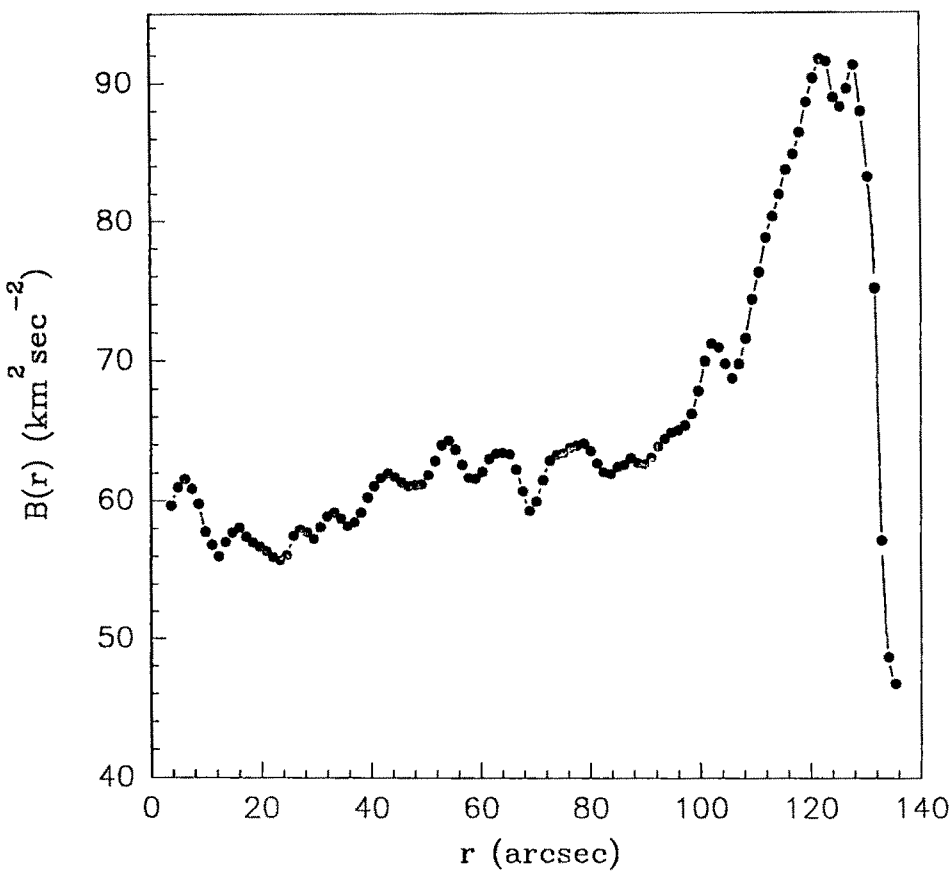

Figure 4.20: Structure function around 2 arc min of θ^1 C Ori for broad component. The standard deviation in each data point corresponds to $\sim \pm 12$ km/s.

artifact.

Around θ^2 A Ori

Structure function was computed for a region of about 120″ around $\theta^2 A$ Ori. Figs. 4.21 & 4.22 show the results obtained for the two components of the velocity field. One can find that there is an irregular behaviour for both the components. Earlier studies of Castañeda (1988) made around this region also showed a similar behavior. However, our data, even though lacks higher spatial resolution, are much more extended and more in number than those of Castañeda's.

Discussion

The most striking difference between the results of Castañeda's (1988) and the present results is in the index. While Castañeda obtains an index which is in line with Kolmogorov's theory, we get an index close to 1, quite in disagreement with the theory. While Castañeda has a better spatial resolution (1″) than ours (4″), our data encompasses the regions around θ^1 C Ori and θ^2 A Ori in a more uniform manner with more number of points than in Casteñeda's work. Further, our data has a velocity resolution of 6 km/s and velocity accuracy of 2 km/s while Castañeda's data has a velocity resolution of $\sim$ 1 km/s. One notices also that Castañeda proposes multiple slopes indicating that the energy is input at different spatial scales.

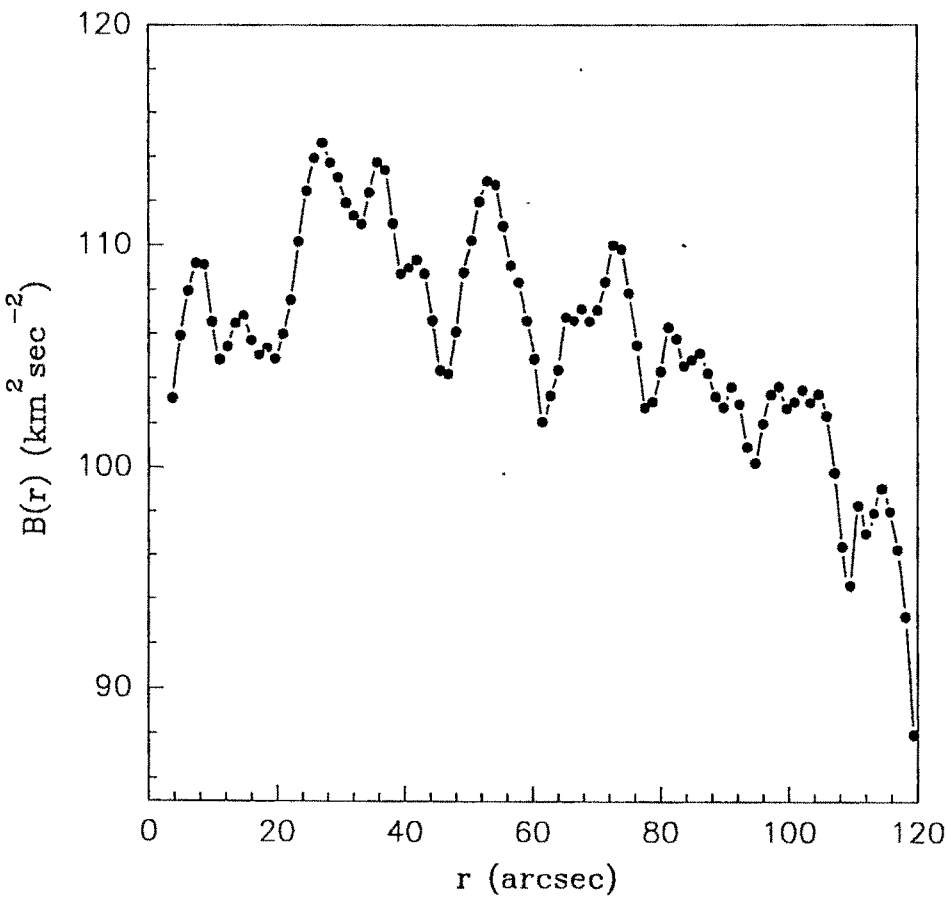

Figure 4.21: Structure function around 2 arc min of θ^2 A Ori for narrow component. The standard deviation in each data point corresponds to $\sim \pm 12$ km/s.

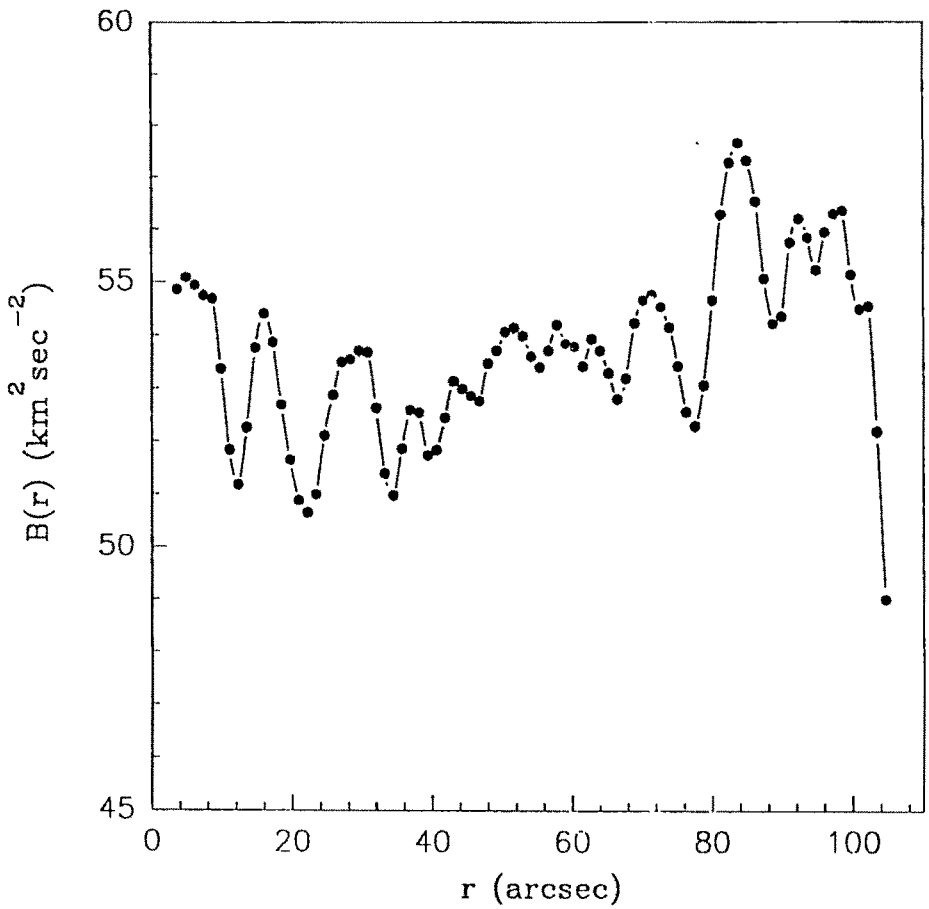

Figure 4.22: Structure function around 2 arc min of θ^2 A Ori for broad component. The standard deviation in each data point corresponds to $\sim \pm 12$ km/s.

In contrast our results lead to a single slope upto about 100″. The failure to satisfy Kolmogorov's law could probably be due to the departure from the physical conditions assumed in the theory of the turbulence. Since the conditions of isotropicity and homogeneity were approximately satisfied by considering a small region, it is possible that the condition of fluid incompressibility may not be satisfied. Similar results were reported by Joncas & Roy (1985) for the nebula $S142$ where it was proposed that compressibility in the fluid could act as a dissipation mechanism and could be responsible for the steeper slope than predicted by Kolmogorov's theory. It was suggested (Lighthill, 1955) that the influence of the compressibility could cause constant radiation of heat from the fluid in the form of sound waves which will subsequently transform into heat.

In order that the turbulence be maintained in the nebula, it requires a constant driving mechanism. It was pointed out that the Kelvin-Helmholtz (K-H) instabilities could be the energy source for turbulence in the HII regions (e.g., Roy and Joncas, 1985). Since the expansion of the ionized gas into the surrounding medium due to the champagne flow takes place with the development of a shock wave, there are possibilities of the growth of K-H instabilities in the Orion nebula as suggested by Blake (1972) and Norman et al (1982). When the shocked gas interacts with the interstellar medium, it gives rise to Rayleigh Taylor (R-T) and K-H instabilities. A R-T instability driven by buoyancy, develops over the front surface of a shock discontinuity whereas the K-H instability driven by shear, develops along the sides of a

shock discontinuity (Fig. 4.23) driven by the flow of the shocked medium over the surface. In a K-H instability, velocity shear is generated at the interface between two uniformly flowing layers of fluid (the expanding ionized matter in the shock and the compressed matter at the shock interface). The resultant mixing gives rise to vortices. The K-H waves arise towards the front and propagate back into the tail. After the waves have grown sufficiently, the shearing of the wave takes place which leads to vorticity. Intense small scale turbulence is generated between the vorticity leading to turbulent cascade process. In order to know whether K-H waves are a viable driving mechanism for turbulence, their growth time has to be found. The growth time of the waves in the absence of magnetic field in an incompressible fluid can be evaluated from the relation given by Blake (1972).

$$t = \left[\frac{k^2\rho_1\rho_2 v^2 \cos^2\theta \ \cos^2\phi}{(\rho_1 + \rho_2)^2} + \left(\frac{\rho_1 - \rho_2}{\rho_1 + \rho_2}\right) gkcos\,\theta\right]^{\frac{1}{2}} \tag{4.6}$$

where ρ_1 and ρ_2 are, respectively, the densities of the intercloud medium and HII region; v is the velocity of the champagne flow; ϕ is the half-cone angle of the champagne flow and θ is the angle between the normal to the surface of the ionized gas flow and the normal to the cone axis; g is the acceleration of the flow and k is the wavenumber of the largest instability. Taking the densities to be 1250 cm^{-3} and 1600 cm $^{-3}$ for the inter-cloud and the ionized regions from Pogge et al (1992), and an average speed of 10 km/s from our observations and the maximum wavelength of 0.223 pc (from Fig. 4.19, the linear portion), $g = 8.65 \times 10^{-6}$ cm sec^{-2} and $\theta = 90°$, the growth time was evaluated. It was found that the first term in eqn. 4.6 becomes negligible

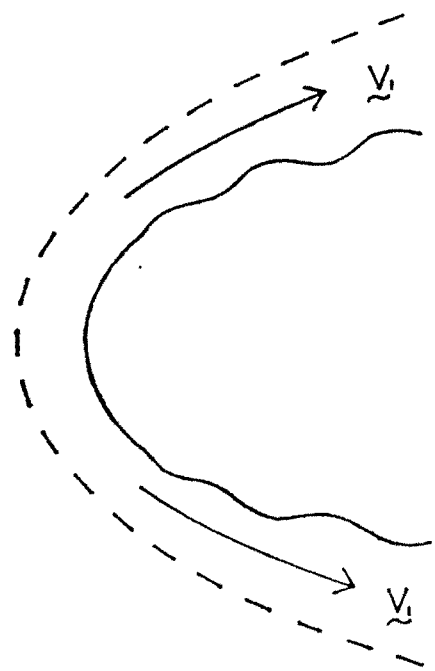

Figure 4.23: Kelvin-Helmholtz instability over the sides of a shock front. V_l denotes the flow speed (adapted from Blake, 1972).

compared to the second term and therefore is neglected. The time required for the growth of the instability was about 1.9×10^4 yrs which is less than the age of the nebula 10^6yr (Massey and Meaburn, 1993). Therefore it implies that the Orion nebula could be in a turbulent state in 1.9×10^4 yrs after the HII region has fully developed and the driving mechanism for turbulence could possibly be the K-H instability. However, it should be mentioned that the estimate was based on the assumption that the fluid is incompressible, while, in reality, it is compressible.